A BIDIRECTIONAL ANTENNA USING A PROBE EXCITED RING

SOMPOL KOSULVIT

A THESIS SUBMITTED IN PARTIAL FULFILLMENT OF
THE REQUIREMENT FOR THE DEGREE
DOCTOR OF ENGINEERING IN ELECTRICAL ENGINEERING
SCHOOL OF GRADUATE STUDIES
KING MONGKUT'S INSTITUTE OF TECHNOLOGY LADKRABANG
2001

ISBN 974-648-374-9

หัวข้อวิทยานิพนธ์	**สายอากาศสองทิศทางที่ใช้โพรบล้อมรอบวงแหวน**
นักศึกษา	**นายสมผล โกศัลวิตร์**
รหัสประจำตัว	38621005
ปริญญา	**วิศวกรรมศาสตรดุษฎีบัณฑิต**
สาขาวิชา	**วิศวกรรมไฟฟ้า**
พ.ศ.	2544
อาจารย์ผู้ควบคุมวิทยานิพนธ์	**รศ.ดร.โมไนย ไกรฤกษ์**
อาจารย์ผู้ควบคุมวิทยานิพนธ์ร่วม	**ศ.ดร.โตชิโอะ วาคาบายาชิ**

บทคัดย่อ

วิทยานิพนธ์ฉบับนี้นำเสนอสายอากาศชนิดที่มีการแพร่กระจายคลื่นสองทิศทางที่มีโครงสร้างประกอบด้วยวงแหวนสี่เหลี่ยมและวงกลมล้อมรอบโพรบที่ป้อนสัญญาณ ได้ทำการวิเคราะห์การแพร่กระจายคลื่นที่เกิดจากวงแหวนสี่เหลี่ยมโดยใช้การแปลงฟูริเยร์ของสนามที่ช่องเปิดสี่เหลี่ยม ซึ่งพิสูจน์นิพจน์ของสนามดังกล่าวมาจากสนามแม่เหล็กไฟฟ้าที่เกิดภายในวงแหวนโดยใช้ฟังก์ชันของกรีนชนิดไดแอดิกเข้าช่วย จากนั้นได้หาอิมพีแดนซ์ของสายอากาศโดยใช้วิธีแรงเคลื่อนไฟฟ้าเหนี่ยวนำ สำหรับสายอากาศที่มีลักษณะโครงสร้างเป็นวงแหวนวงกลม จะหาค่าสนามบริเวณช่องเปิดที่ระยะห่างจากโพรบป้อนสัญญาณพอเหมาะที่ทำให้เกิดโหมดพื้นฐานเท่านั้น และจากนั้นจึงได้ทำการหาสนามที่แพร่กระจายออกจากสายอากาศ จากการคำนวณพบว่า ที่สภาวะที่เหมาะสมที่สุดที่ได้ทำการวิเคราะห์ สายอากาศจะมีการแพร่กระจายคลื่นเป็นลักษณะสองทิศทางที่มีค่าสภาพเจาะจงทิศทางมากกว่า *6* dBi ตลอดช่วงกว้างความถี่ใช้งานมากกว่า *10* เปอร์เซ็นต์ จากการทดสอบคุณสมบัติของสายอากาศที่กล่าวมาทั้งหมดนี้พบว่า สายอากาศชนิดนี้เหมาะสมสำหรับการประยุกต์ใช้เป็นสายอากาศของสถานีฐานในระบบการสื่อสารเคลื่อนที่ที่มีบริเวณให้บริการในลักษณะแคบตามแนวยาว

Thesis Title	A Bidirectional Antenna Using a Probe Excited Ring
Student	Mr. Sompol Kosulvit
Student ID.	38621005
Degree	Doctor of Engineering
Programme	Electrical Engineering
Year	2001
Thesis Advisor	Assoc. Prof. Dr. Monai Krairiksh
Co-advisor	Prof. Dr.Toshio Wakabayashi

ABSTRACT

This thesis concerns about the study of characteristics of structures consisting of a probe that is used to excite rectangular and circular rings. Radiated field of the rectangular ring is analyzed from the Fourier transform of the aperture field which is derived from the field inside the ring by using Dyadic Green's function. The impedance of this antenna is derived by using induced EMF method. For the circular ring, the aperture field is determined by a proper distance from the probe that provides only the field distribution of dominant mode. Then, the radiated field can be obtained. From the numerical results, it was pointed out that, at an optimal dimension, these antennas yield the bidirectional pattern with directivity in excess of *6* dBi over *10%* bandwidth. This characteristic is validated by experiments and found that it is essential for being employed as a base-station antenna of a mobile communication system in a narrow service area.

Acknowledgements

I would like to express my profound gratitude to Associate Professor Monai Krairiksh and Professor Toshio Wakabayashi, the co-advisors, for their continuous guidance and encouragement throughout the project.

Professor Sittichai Pookaiyaudom, President of Mahanakorn University of Technology, is highly appreciated for his continuous support.

I am particularly grateful to Professor Wiwat Kiranon for his helpful discussion.

Mr. Chuwong Phongcharoenpanich and all the graduate students in the Wireless Communication Laboratory are acknowledged for their support.

I wish to thank the Japan International Cooperation Agency (JICA) for its funding to present the results in the 1999 International Conference on Microwave and Millimeter Wave Technology.

Sompol Kosulvit

Table of Contents

Table of Contents (continue)

Page

List of Tables

List of Figures

List of Figures (continue)

Chapter 1
Introduction

1.1 Rationale

At present, cellular mobile system has played a vital role and it has become an important part of daily life [1]. The number of subscribers have been increased drastically, and microcellular systems have been applied successfully. Hence, the number of base stations are very large. Therefore, developments of the cost-effective base-station antennas are of importance. Generally, the omnidirectional antenna is employed to cover the approximated circular area. However, on the long and narrow path service areas such as highway, tunnel, and corridor; the bidirectional antenna is installed in place of the omnidirectional one. If the antenna pattern can be restricted to the narrow path, the coverage area can be enhanced. The conventional bidirectional antennas are made by combining two unidirectional antennas, such as Yagi, pointed in opposite directions or the omnidirectional antennas such as monopoles excited by appropriate phase [2]. The antenna constructed by this technique suffers from feeder loss and complicated structure that makes it expensive. Thus, many researches and developments on bidirectional antenna have been continuously conducted. Some of works are cited as the following literature.

The bidirectional narrow patch antenna (BNPA), which has narrow patches on both sides of a narrow dielectric substrate fed by a parallel striplines, is easily fabricated by printing patches and feeding network on a substrate. Unfortunately, it has low radiation efficiency. By adding two opposing parasitic patches to a BNPA to form the so-called BNPA-A, the radiation efficiency can be improved [3]. It was found that gain is higher than a collinear antenna of the same length. For a wide street about the width

ranging from *30* to *60* meters, the BNPA element is developed to be a bidirectional rod antenna (BIRA) that possesses an optimum beam shape [4]. Another development of a bidirectional antenna is to use two notch antennas cut in a sheet of conductor above a ground plane. It was proposed to extend the coverage of a relay station in booster system inside tunnel [5]. Cross polarization is undesirable and it needs to be suppressed in the H-plane of this notch antenna. It can be carried out by using the crank shaped antenna, which is modified from the original notch antenna [6]. It was found that the radiation patterns of these antennas are tilted up from the mounting wall and they should be tilted downward in order to cover the service area. This was accomplished by using the crank shaped antenna with the parasitic elements for gain enhancement [7]. From these aforementioned literatures, it is evident that development of a bidirectional antenna that has suitable characteristics for a particular application is desired. Moreover, cost effectiveness must be considered since the number of cells are very large.

According to the requirement of cost effective bidirectional antenna, the use of a ring to surround a monopole is proposed. In this regard, it is expected that an omnidirectional pattern can be modified to a bidirectional one. However, it is necessary to know an appropriate dimension of the ring that provides the desirable characteristics, i.e., maximum gain, compact structure and particularly low cost. Therefore, investigation from a simple mathematical model was initiated. A monopole surrounded by a rectangular ring was modeled to investigate its characteristics by using Dyadic Green's function. Once the radiated field from this structure is obtained, radiation characteristics can be analyzed. Then, the optimum dimension that provides maximum gain with compact size is achieved. Furthermore, impedance characteristic is investigated to match the antenna with the transmission line. Although the rectangular structure is simple for modeling, practically it is found that the circular structure is more interesting. It can be mass produced

conveniently. Hence, the second approach is to apply the principle from the rectangular structure to investigate the circular structure. It is evident that the bidirectional antenna using a probe excited circular ring can be designed and it provides the satisfactory characteristics, both technically and economically.

1.2 Scope of the Thesis

To fulfill the purpose of this thesis, numerous works must be carried out both theoretically and experimentally. They are summarized as follow:

Chapter 2 introduces the model of the bidirectional antenna using a probe excited rectangular ring. The aperture field at the two ends of the ring is derived from the field inside the ring, with the feed probe excited in it. This is carried out by integrating the Dyadic Green's function and the probe current. Then the radiated field is calculated from the apertures using Huygen's principle. Finally, superposition of the fields from the two apertures are performed to investigate the radiation characteristics, i.e., radiation patterns and directivity. Input impedance of the probe excited rectangular ring is derived by using induced EMF method. The input impedance of this antenna is represented as the reciprocal of a shunt admittance of the probe in a ring, regardless of reflection, and two aperture admittances. Then VSWR of this antenna is calculated to estimate its matching condition.

Chapter 3 presents the analytical results of a bidirectional antenna using a probe excited rectangular ring. Aperture distribution, radiation patterns, directivity and impedance are analyzed in terms of antenna parameters, such as ring width, ring height, ring length and probe length. These results are shown in figures and variations of their characteristics on frequency are also discussed.

Chapter 4 applies the analytical results in chapter 3 to design a bidirectional antenna that maximum gain can be achieved by using the shortest ring length. The appropriate probe length is chosen to obtain the lowest VSWR. Validation of the model of the antenna was conducted by comparing the calculation with the measured results. Experimental results such as radiation patterns, impedance and gain are illustrated.

Chapter 5 introduces a bidirectional antenna using a probe excited circular ring by applying the principle of a rectangular structure one. Its characteristics are also illustrated in this chapter.

Chapter 6 addresses the design procedure of the bidirectional antenna using a probe excited circular ring in addition to the experimental results. Experimental data when the antenna is used as a base station of a Personal Communication Telephone (PCT) on an elevated high way are shown.

Chapter 7 summarizes the consequence of the preceding chapters together with the discussion of the future studies.

Chapter 2
Formulations of a Bidirectional Antenna Using a Probe Excited Rectangular Ring

2.1 Introduction

Radiation characteristics such as radiation pattern and directivity are essential in wireless communication. The former is used in antenna installation whereas the latter contributes to the communication range. To investigate radiation characteristics of a bidirectional antenna using a probe excited rectangular ring, the aperture fields at both ends on the ring are derived from the field inside it by using the Dyadic Green's function. This function is derived in the series from. Then, the radiated field is calculated from the aperture using Huygen's principle. Finally, superpositions of the fields from the two apertures are performed. Furthermore, impedance of the antenna must be matched to the transceiver system. Hence, it must be clarified. This chapter describes the procedure to analyze the radiation and impedance characteristics of this antenna.

2.2 Dyadic Green's function of the Structure

Green's function derived here is for infinite waveguide. It is assumed that the aperture are perfectly radiated into space therefore the Green's function derived here can be applied. A bidirectional antenna using a probe excited rectangular ring consists of a linear probe of length l aligned along the y axis. This probe is surrounded by a conducting rectangular ring that the surface is represented by, $(-a/2 \le x \le a/2, y = -b/2, -c/2 \le z \le c/2)$, $(-a/2 \le x \le a/2, y = b/2, -c/2 \le z \le c/2)$, $(x = -a/2, -b/2 \le y \le b/2, -c/2 \le z \le c/2)$, $(x = a/2, -b/2 \le y \le b/2, -c/2 \le z \le c/2)$. At the ends of the ring, there are two apertures

on the planes $z = -c/2$ and $z = c/2$, respectively. The geometry of the antenna is shown in Fig. 2.1

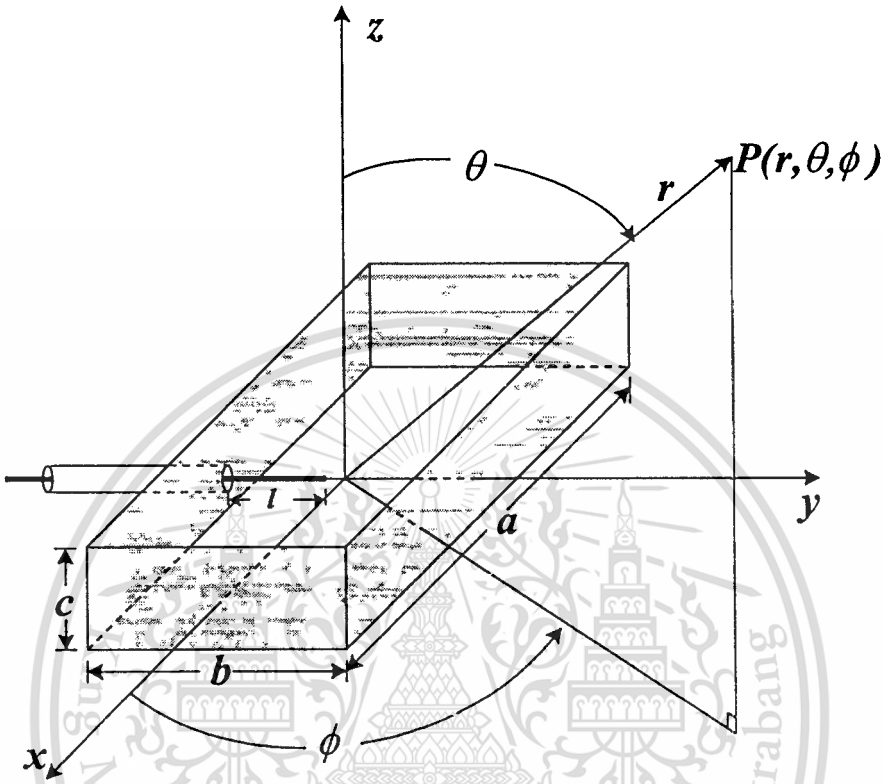

Fig. 2.1 A probe excited rectangular ring

To estimate antenna characteristics, electromagnetic fields inside the ring must be firstly calculated. The Dyadic Green's function, a response at an observer from the unit point source, is a powerful tool to obtain the electromagnetic field in the source region. The vector wave equation, in rectangular coordinate, is represented as [8]-[9]

$$\nabla^2 \overline{E}(x,y,z) + k^2 \overline{E}(x,y,z) = j\omega\mu \overline{J}(x,y,z) \qquad (2.1)$$

subject to the boundary condition that tangential electric field on the conducting ring surface is vanished such that

$$E_x(-a/2 \le x \le a/2,\ y=-b/2,\ -c/2 \le z \le c/2)$$
$$= E_x(-a/2 \le x \le a/2,\ y=b/2,\ -c/2 \le z \le c/2) = 0 \quad (2.2a)$$
$$E_y(x=-a/2,\ -b/2 \le y \le b/2,\ -c/2 \le z \le c/2)$$
$$= E_y(x = a/2,\ -b/2 \le y \le b/2,\ -c/2 \le z \le c/2) = 0 \quad (2.2b)$$
$$E_z(x=-a/2,\ -b/2 \le y \le b/2,\ -c/2 \le z \le c/2)$$
$$= E_z(x= a/2,\ -b/2 \le y \le b/2,\ -c/2 \le z \le c/2)$$
$$= E_z(-a/2 \le x \le a/2,\ y=-b/2,\ -c/2 \le z \le c/2)$$
$$= E_z(-a/2 \le x \le a/2,\ y=b/2,\ -c/2 \le z \le c/2) = 0 \quad (2.2c)$$

Since the probe (in Fig.2.1) is oriented in the y direction, therefore $\bar{J}(x',y',z')$ is represented by $\bar{J}_y(x',y',z')$, k is the phase constant of the field within the ring, ω denotes the angular frequency and μ is the permeability of the medium. In this problem, free space is considered. The wave is assumed to be a traveling wave in both $+z$ and $-z$ directions. The time-harmonic variations are of $e^{+j\omega t}$, and they are suppressed.

The Dyadic Green's function is the response from the unit point source which can be represented by delta function δ. It consists of nine components, i.e., G_{xx}, G_{xy}, G_{xz}, G_{yx}, G_{yy}, G_{yz}, G_{zx}, G_{zy}, G_{zz}. In case of G_{yy}, for instance, it must satisfy the partial differential equation

$$\nabla^2 G_{yy}(x,y,z;x',y',z') + k^2 G_{yy}(x,y,z;x',y',z') = \delta(x-x')\delta(y-y')\delta(z-z') \quad (2.3)$$

subject to the boundary condition

$$G_{yy}(x = -a/2,\ -b/2 \le y \le b/2,\ -c/2 \le z \le c/2)$$
$$= G_{yy}(x = a/2,\ -b/2 \le y \le b/2,\ -c/2 \le z \le c/2) = 0 \quad (2.4)$$

where $G_{yy}(x;y,z;x',y',z')$ denotes the y component of Dyadic Green's function at the observation point (x,y,z) due to the point source oriented along y direction located at (x',y',z').

The Dyadic Green's function derived in the series form, by assuming its solution, can be represented by a two-function Fourier series of cosine function in x and y. They satisfy, respectively, the boundary condition at x = $-a/2$ and $a/2$. Thus we can express $G_{yy}(x,y,z;x',y',z')$ as

$$G_{yy}(x,y,z;x',y',z') = \sum_{m=0}^{\infty}\sum_{n=0}^{\infty} g_{mn}(z;x',y',z')\sin\left(\frac{m\pi(x+a/2)}{a}\right)\cos\left(\frac{n\pi(y+b/2)}{b}\right) \quad (2.5)$$

g_{mn} is the Fourier coefficient. It is noted that m and n cannot be concurrently zero since the null mode will be occurred.

Substituting (2.5) in (2.3) leads to

$$\sum_{m=0}^{\infty}\sum_{n=0}^{\infty}\left[-\left(\frac{m\pi}{a}\right)^2-\left(\frac{n\pi}{b}\right)^2+k^2+\frac{\partial^2}{\partial z^2}\right]g_{mn}(z;x',y',z')\times \sin\left(\frac{m\pi(x+a/2)}{a}\right)\cos\left(\frac{n\pi(y+b/2)}{b}\right)=\delta(x-x')\delta(y-y')\delta(z-z') \quad (2.6)$$

Multiplying both sides of (2.6) by $\sin\left(\frac{m\pi(p+a/2)}{a}\right)\cos\left(\frac{n\pi(q+b/2)}{b}\right)$, integrating between $-a/2$ to $a/2$ in x and $-b/2$ to $b/2$ in y, and using the relation that

$$\int_{-a/2}^{a/2}\cos^2\left(\frac{m\pi}{a}x\right)dx=\begin{cases}a/2\,; m\neq 0\\ a\quad ; m=0\end{cases} \quad (2.7)$$

we can reduce (2.6) to

$$\left(\frac{d^2}{dz^2}+k_z^2\right)g_{mn}(z;x',y',z')=\frac{4}{ab}\sin\left(\frac{m\pi(x'+a/2)}{a}\right)\cos\left(\frac{n\pi(y'+b/2)}{b}\right)\delta(z-z') \quad (2.8)$$

where

$$k_z^2=k^2-\left[\left(\frac{m\pi}{a}\right)^2+\left(\frac{n\pi}{b}\right)^2\right]$$

$$=k^2-\left(k_x^2+k_y^2\right)$$

$$k_x=\frac{m\pi}{a};\ m=0,1,\ldots$$

$$k_y=\frac{n\pi}{b};\ n=0,1,\ldots$$

g_{mn} can be written as [10]

$$g_{mn}(z;x',y',z')=\begin{cases}j\dfrac{2}{ab}\dfrac{\sin\left(\frac{m\pi(x'+a/2)}{a}\right)\cos\left(\frac{n\pi(y'+b/2)}{b}\right)e^{-jk_z(z'-z)}}{k_z};\ z<z'\\ j\dfrac{2}{ab}\dfrac{\sin\left(\frac{m\pi(x'+a/2)}{a}\right)\cos\left(\frac{n\pi(y'+b/2)}{b}\right)e^{-jk_z(z-z')}}{k_z};\ z\geq z'\end{cases} \quad (2.9a)$$

Consequently, the Dyadic Green's function G_{yy} can be expressed as

$$G_{yy}(x,y,z;x',y',z')=j\frac{2}{ab}\sum_{m=0,1,\ldots}^{\infty}\sum_{n=0,1,\ldots}^{\infty}\frac{1}{k_z}\sin\left(\frac{m\pi(x'+a/2)}{a}\right)\cos\left(\frac{n\pi(y'+b/2)}{b}\right)$$
$$\times\sin\left(\frac{m\pi(x+a/2)}{a}\right)\cos\left(\frac{n\pi(y+b/2)}{b}\right)e^{-jk_z|z-z'|} \quad (2.10a)$$

By following the same procedure described above, G_{xy} and G_{zy} are expressed as follows:

$$G_{xy}(x,y,z;x',y',z') = j\frac{2}{ab}\sum_{m=0,1,\ldots}^{\infty}\sum_{n=0,1,\ldots}^{\infty}\frac{1}{k_z}\cos\left(\frac{m\pi(x'+a/2)}{a}\right)\sin\left(\frac{n\pi(y'+b/2)}{b}\right) \times\cos\left(\frac{m\pi(x+a/2)}{a}\right)\sin\left(\frac{n\pi(y+b/2)}{b}\right)e^{-jk_z|z-z'|} \quad (2.10b)$$

$$G_{zy}(x,y,z;x',y',z') = j\frac{2}{ab}\sum_{m=0,1,\ldots}^{\infty}\sum_{n=0,1,\ldots}^{\infty}\frac{1}{k_z}\sin\left(\frac{m\pi(x'+a/2)}{a}\right)\sin\left(\frac{n\pi(y'+b/2)}{b}\right) \times\sin\left(\frac{m\pi(x+a/2)}{a}\right)\sin\left(\frac{n\pi(y+b/2)}{b}\right)e^{-jk_z|z-z'|} \quad (2.10c)$$

We have shown only three components of Dyadic Green's function since the problem under consideration has only the current along the y direction.

2.3 Field in a Rectangular Ring

The electric field of a probe excited rectangular ring is obtained by integrating the Dyadic Green's function as derived in the previous section with the current on the probe. It can be represented as follow:

$$\begin{aligned}\bar{E}(x,y,z) &= j\omega\mu\iiint_{V}\bar{\bar{G}}(x,y,z;x',y',z')\cdot\bar{J}(x',y',z')\,dx'dy'dz' \\ &= j\omega\mu\int_{-b/2}^{l-b/2}\bar{\bar{G}}(x,y,z;x',y',z')\cdot J_y(y')\hat{a}_y dy'\end{aligned} \quad (2.11)$$

Since the diameter of the probe is small compared with the wavelength, the sinusoidal current distribution on the probe can be reasonably assumed as

$$J_y(x',y',z') = J_y(y') = J_m\sin[k(l-y'-b/2)] \quad (2.12)$$

where $J_y(x',y',z')$ is the current distribution on the probe along the y axis and J_m is the maximum current.

By substituting the Dyadic Green's function in (2.10a) – (2.10c) and current distribution in (2.12) into (2.11), the resultant electric field can be expressed as

$$E_x(x,y,z) = -\frac{\omega\mu J_m}{ab}\sum_{m=0,1,\ldots}^{\infty}\sum_{n=0,1,\ldots}^{\infty}\frac{e^{-jk_z|z-z'|}}{k_z}\cos\left(\frac{m\pi}{2}\right)\cos\left(\frac{m\pi(x+a/2)}{a}\right)\sin\left(\frac{n\pi(y+b/2)}{b}\right) \times\left\{\frac{1}{X}\left[\sin\left(\frac{n\pi l}{b}\right)-\sin(kl)\right]+\frac{1}{Y}\left[\sin\left(\frac{n\pi l}{b}\right)+\sin(kl)\right]\right\} \quad (2.13a)$$

$$E_y(x,y,z) = -\frac{\omega\mu J_m}{ab}\sum_{m=0,1,\ldots}^{\infty}\sum_{n=0,1,\ldots}^{\infty}\frac{e^{-jk_z|z-z'|}}{k_z}\sin\left(\frac{m\pi}{2}\right)\sin\left(\frac{m\pi(x+a/2)}{a}\right)\cos\left(\frac{n\pi(y+b/2)}{b}\right) \times\left\{\frac{1}{X}\left[\cos\left(\frac{n\pi l}{b}\right)-\cos(kl)\right]+\frac{1}{Y}\left[\cos\left(\frac{n\pi l}{b}\right)-\cos(kl)\right]\right\} \quad (2.13b)$$

$$E_z(x,y,z) = -\frac{\omega\mu J_m}{ab}\sum_{m=0,1,\ldots}^{\infty}\sum_{n=0,1,\ldots}^{\infty}\frac{e^{-jk_z|z-z'|}}{k_z}\sin\left(\frac{m\pi}{2}\right)\sin\left(\frac{m\pi(x+a/2)}{a}\right)\sin\left(\frac{n\pi(y+b/2)}{b}\right) \times\left\{\frac{1}{X}\left[\sin\left(\frac{n\pi l}{b}\right)-\sin(kl)\right]+\frac{1}{Y}\left[\sin\left(\frac{n\pi l}{b}\right)+\sin(kl)\right]\right\} \quad (2.13c)$$

$$\bar{E} = E_x\hat{a}_x + E_y\hat{a}_y + E_z\hat{a}_z \quad (2.13d)$$

where $X = k-\frac{n\pi}{b}$ and $Y = k+\frac{n\pi}{b}$.

It should be pointed out that the proposed structure has E_x and E_y which contribute to the radiation, but E_x has very low coefficient compared to E_y. Hence, it is obvious that only E_y is the component that radiates. E_z

does not contribute to the radiation since its direction is normal to the aperture.

2.4 Aperture Distribution

Electric field distribution in a rectangular ring is expressed in (2.13d) in the above section. In order to calculate the radiation field from the apertures of the rings, the aperture field must be known. It can be obtained by calculating the field at the apertures ($z = \pm\frac{c}{2}$). Hence

$$E_y = -\frac{\omega\mu J_m}{ab}\sum_{m=0,1,\ldots}^{\infty}\sum_{n=0,1,\ldots}^{\infty}\frac{e^{-j\frac{k_z c}{2}}}{k_z}\sin\left(\frac{m\pi}{2}\right)\sin\left(\frac{m\pi(x+a/2)}{a}\right)\cos\left(\frac{n\pi(y+b/2)}{b}\right) \times\left\{\left(\frac{X+Y}{XY}\right)\left[\cos\left(\frac{n\pi l}{b}\right)-\cos(kl)\right]\right\} \quad (2.14)$$

2.5 Radiated Field

According to the antenna structure shown in Fig.2.1, the field is considered to be radiated from the apertures at the two ends of the ring. On these apertures, the radiated field is equal to the aperture tangential field. If the apertures are assumed to be on the $z = 0$ plane, the radiated field, which is a two-dimensional Fourier transform of the aperture field [11], can be expressed as

$$\bar{E}(\bar{r}) = jk\frac{e^{-jkr}}{2\pi r}\left[\left(f_x\cos\phi + f_y\sin\phi\right)\hat{a}_\theta + \left(f_y\cos\phi - f_x\sin\phi\right)\cos\phi\hat{a}_\phi\right] \quad (2.15)$$

where f_x and f_y are the x and y components of the Fourier transform of the aperture field. Since the probe is oriented along the y axis, there is only the f_y existing in (2.15). Therefore, (2.15) becomes

$$\overline{E}(\overline{r}) = jk\frac{e^{-jkr}}{2\pi r}\left[f_y \sin\phi \hat{a}_\theta + f_y \cos\phi \hat{a}_\phi\right], \qquad (2.16)$$

where

$$f_y(k_x,k_y) = -\frac{j\omega\mu J_m}{4}\sum_{m=0,1,\ldots}^{\infty}\sum_{n=0,1,\ldots}^{\infty}\frac{e^{-j\frac{k_z c}{2}}}{k_z}\sin^2\left(\frac{m\pi}{2}\right)\cos\left(\frac{n\pi}{2}\right)\left\{\left(\frac{X+Y}{XY}\right)\left[\cos\left(\frac{n\pi l}{b}\right)-\cos(kl)\right]\right\}$$
$$\times\left\{Sa\left(\frac{k_x a+m\pi}{2}\right)-Sa\left(\frac{k_x a-m\pi}{2}\right)\right\}\left\{Sa\left(\frac{k_y b+n\pi}{2}\right)+Sa\left(\frac{k_y a-n\pi}{2}\right)\right\} \qquad (2.17)$$

and $Sa(x)=\frac{\sin x}{x}$, $k_x = k\sin\theta\cos\phi$, $k_y = k\sin\theta\sin\phi$.

The radiated field in (2.16) was derived when the aperture is located on the $z = 0$ plane. When the apertures are removed from the $z = 0$ plane to $z = \pm c/2$, the radius r is substituted by r_1 and r_2, respectively as represented in Fig. 2.2 These radii, r_1 and r_2, can be approximated [12], respectively, as follows: $r_1 \approx r - \frac{c}{2}\cos\theta$ and $r_2 \approx r + \frac{c}{2}\cos\theta$ for phase variation and $r_1 \approx r_2 \approx r$ for amplitude variation.

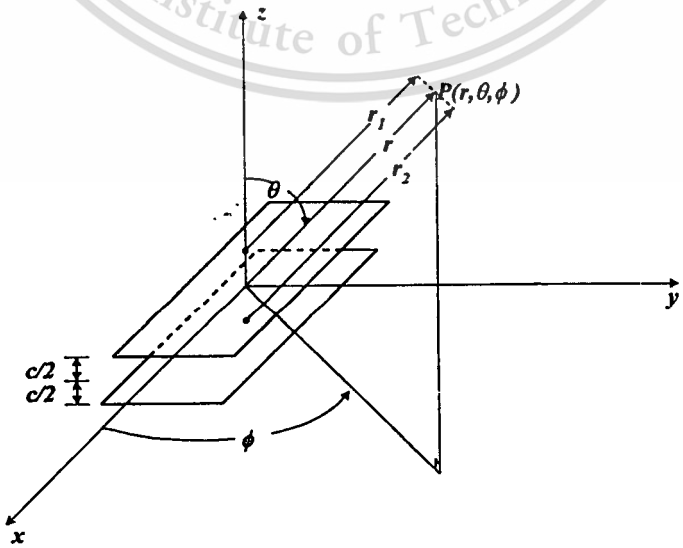

Fig. 2.2 Far-field observation of the two apertures

The far field pattern of the antenna can be expressed by neglecting mutual coupling, as a superposition of the fields from these two apertures. Since the fields radiated from the two apertures have the same phase but in opposite directions; therefore, as they are combined, the resultant field can be written as

$$\overline{E}_t(\bar{r}) = \overline{E}(\bar{r}) \cdot 2\sin\left[\frac{1}{2}(kc\cos\theta + k_z c)\right] \tag{2.18}$$

In the far field region electric field and magnetic field are related by the intrinsic impedance (η) such that

$$\eta = \frac{|\overline{E}|}{|\overline{H}|} \tag{2.19}$$

2.6 Directivity

Directivity is a Figure of Merit which presents the ability of the antenna that can direct electromagnetic wave to a particular direction. It is expressed as a ratio of maximum radiation intensity of the unknown antenna to that of an isotropic one. Directivity can be written in mathematical form as

$$D_0 = \frac{U_{max}}{U_0}$$

$$= \frac{4\pi U_{max}}{P_{rad}} \tag{2.20}$$

where D_0 is directivity (dimensionless), U_{max} is maximum radiation intensity U_0 is radiation intensity of isotropic radiator and P_{rad} is radiated power.

Since U is calculated from average power density (W_{av}) by using [12]

$$U = r^2 W_{av} \tag{2.21}$$

where r is the radius distance from the antenna to the observation point and W_{av} is average power density. It can be expressed as

$$\overline{W}_{av} = W_{av}\hat{a}_w = \frac{1}{2}\mathrm{Re}(\overline{E} \times \overline{H}^*) \tag{2.22}$$

$\overline{E}$ and $\overline{H}$ in (2.22) are the electric field and magnetic field radiated from the antenna and asterisk (*) indicates the complex conjugate of the field. For the proposed antenna, $\overline{E}$ can be calculated from (2.18) whereas $\overline{H}$ is obtained from (2.19), $\hat{a}_w$ is the unit vector of the wave.

Radiated power (P_{rad}) is represented as the close surface integral of the average power density over any closed surface enclosing antenna such that

$$P_{rad} = \frac{1}{2}\oint \mathrm{Re}[\overline{E} \times \overline{H}^*] \cdot d\overline{S} \tag{2.23}$$

By substituting the maximum value of radiation intensity and radiated power into (2.20), the directivity of the probe excited rectangular ring can be expressed as

$$D_0 = \frac{4\pi\left(|E_\theta|^2 + |E_\phi|^2\right)_{max}}{\int_0^{2\pi}\int_0^{\pi}\left(|E_\theta|^2 + |E_\phi|^2\right)\sin\theta d\theta d\phi} \tag{2.24}$$

2.7 Input Impedance and VSWR

Input impedance of the antenna is considered to be the reciprocal of shunt admittances consisting of admittance of the probe and two aperture admittances.

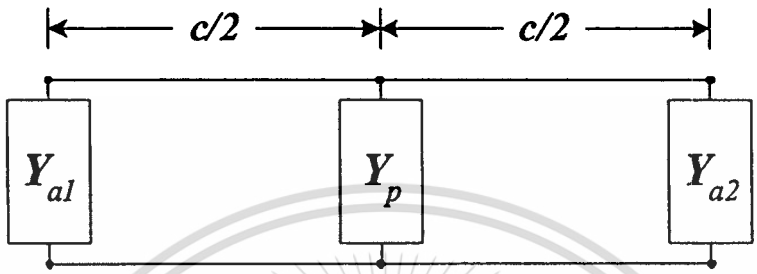

Fig. 2.3 An equivalent circuit.

To find the input impedance of a probe of radius ρ_a, excited rectangular ring, the tangential electric field component on the surface of the probe is calculated from (2.13b). Based on the current distribution and tangential electric field along the surface of the probe, the induced potential developed at the terminal of the probe based on maximum current (V_m) is given by

$$V_m = \int_{-b/2}^{l-b/2} dV_m$$

$$= -\frac{1}{I_m} \int_{b/2}^{l-b/2} J_y(\rho = \rho_a, y = y') E_y(\rho = \rho_a, y = y')\, dy' \qquad (2.25)$$

The input impedance (referred to the current maximum I_m) is defined as

$$Z_p = \frac{V_m}{I_m} \qquad (2.26)$$

and can be expressed as

$$Z_p = -\frac{1}{I_m^2}\int_{-b/2}^{l-b/2} J_y(\rho=\rho_a, y=y')E_y(\rho=\rho_a, y=y')\,dy' \qquad (2.27)$$

I_m is the same as J_m in (2.12)

By substituting electric field from (2.13) and current from (2.12) into (2.27), the input impedance of the probe excited rectangular ring is

$$Z_p = \frac{\omega\mu}{2ab}\sum_{m=0,1,\ldots}^{\infty}\sum_{n=0,1,\ldots}^{\infty}\frac{1}{k_z}\sin^2\left(\frac{m\pi}{2}\right)\left[\left(\frac{X+Y}{XY}\right)\left[\cos\left(\frac{n\pi l}{b}\right)-\cos(kl)\right]\right]^2 \qquad (2.28)$$

The input impedance of the probe excited rectangular ring in (2.28) is calculated based on the maximum current (at the input terminal since maximum current takes place at the input terminal). It is the impedance calculated by assuming that the field is totally radiated from the apertures at the two ends of the ring. However, since there exist the two apertures, they must be taken into account in investigating the input impedance of the antenna.

Aperture admittance (Y_a) can be calculated by using the relation [13]

$$Y_a = \frac{1}{V^2}\int_{-\frac{a}{2}}^{\frac{a}{2}}\int_{-\frac{b}{2}}^{\frac{b}{2}}\left(\overline{E}_t^a \times \overline{H}_t^a\right)\cdot\hat{a}_z\,dydx \qquad (2.29)$$

where E_t^a is the tangential electric field on the apertures. It can be considered from (2.14) whereas H_t^a is the aperture magnetic field which can be derived by substituting E_y from (2.13) into Maxwell's equation (Ampere's

Law). V is the dominant mode voltage coupled to the aperture. After manipulating as described, Y_a can be expressed as

$$Y_a = \frac{1}{V^2}\int_{-\frac{b}{2}}^{\frac{b}{2}}\int_{-\frac{a}{2}}^{\frac{a}{2}} \omega\mu\left(\frac{J_m}{ab}\right)^2\left[\sum_{m=0}^{\infty}\sum_{n=0}^{\infty}\frac{1}{k_z}\sin\left(\frac{m\pi}{2}\right)\sin\left(\frac{m\pi(x+a/2)}{a}\right)\cos\left(\frac{n\pi(y+b/2)}{b}\right)e^{-j\frac{k_z c}{2}}\right.$$
$$\left.\times\left\{\left(\frac{X+Y}{XY}\right)\left[\cos\left(\frac{n\pi l}{b}\right)-\cos(kl)\right]\right\}\right]$$
$$\times\left[\sum_{m=0}^{\infty}\sum_{n=0}^{\infty}\sin\left(\frac{m\pi}{2}\right)\sin\left(\frac{m\pi(x+a/2)}{a}\right)\cos\left(\frac{n\pi(y+b/2)}{b}\right)e^{-j\frac{k_z c}{2}}\right. \qquad (2.30)$$
$$\left.\times\left\{\left(\frac{X+Y}{XY}\right)\left[\cos\left(\frac{n\pi l}{b}\right)-\cos(kl)\right]\right\}\right]dxdy$$

By transforming these admittances, from the ends of the both apertures ($z = \pm c/2$), along the waveguide to the probe position ($z = 0$), the combination of these to apertures admittances and the probe admittances provide the input admittance of the probe excited rectangular ring. Then, the input impedance of this antenna can be found by inversion of this input admittance.

2.8 Conclusion

This chapter introduces the radiation theory of a bidirectional antenna using a probe excited rectangular ring. Starting from the Green's function, the field in the antenna's structure can be investigated. Then, the aperture field can be obtained and is employed to calculate the radiated field and directivity. Finally, directivity is derived. Input impedance is derived by using the induced EMF method. The results from this derivation can be applied in investigation of radiation characteristic of this antenna.

Chapter 3

Analysis of a Bidirectional Antenna Using a Probe Excited Rectangular Ring

3.1 Introduction

Based on the formulations derived in chapter 2, this chapter describes characteristics of a bidirectional antenna using a probe excited rectangular ring. Numerical results to be discussed in this chapter are aperture distribution, radiation pattern, directivity, input impedance and Voltage Standing Wave Ratio (VSWR). From these characteristics, it is possible to find parameters such as probe length, a ring length and so on in order to design and fabricate this antenna.

3.2 Aperture Distribution

According to the total field radiated by this antenna as shown in (2.13)-(2.18), it is obvious that the radiation characteristics of the antenna depend on the following parameters, i.e., the probe length (l), the ring width (a), the ring height (b) and the ring length (c). Since the antenna structure is the same as a rectangular waveguide, in this circumstance the width and the height of the ring are chosen to be the dimension of a standard waveguide operating at a dominant TE_{10} mode. However, if the ring length is short, the field at the aperture which is close to the probe will consist of several modes and the evanescent wave of the higher order modes near the probe still have a significant level. Therefore, they contribute to the aperture field and, consequently, the radiated field. For the waveguide dimension of $a = 0.69\lambda$, $b = 0.35\lambda$, $l=0.28\lambda$, the aperture field distribution of TE_{10} (E_y component), TE_{01} (E_x component) and TE_{30} (E_y component) wave are illustrated in Fig.3.1 (a) –(c) respectively. Also, Fig.3.2 shows the power distribution of each

mode within the ring. As the length c is increased, these higher order modes attenuate rapidly. When the ring length is increased to 0.25λ these higher modes vanish at an expense of the long aperture separation.

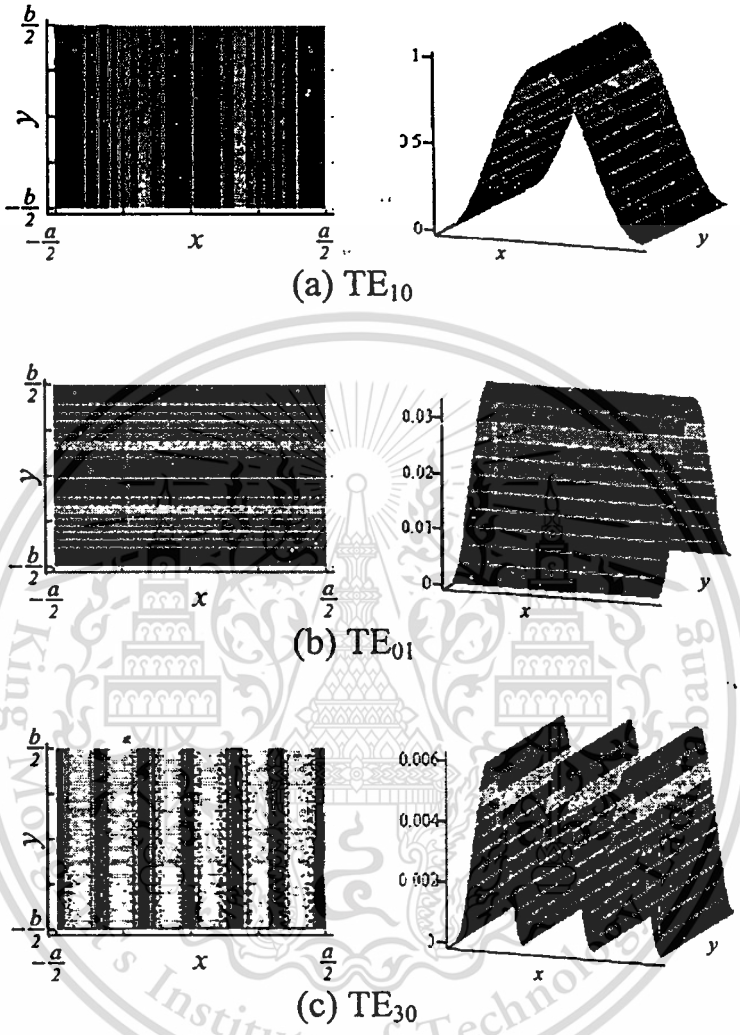

Fig.3.1 Aperture power distribution

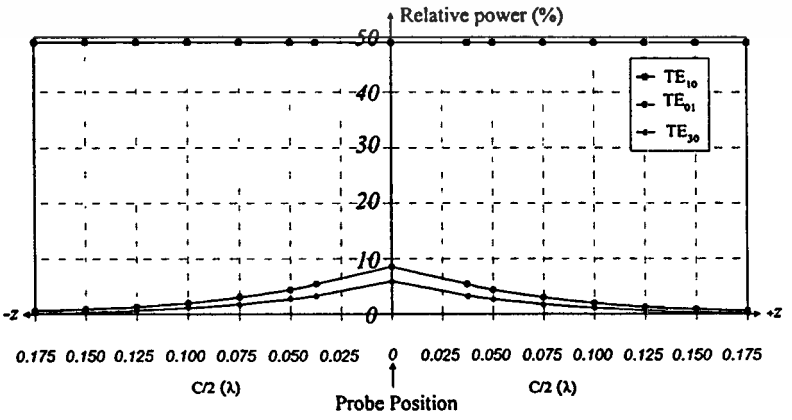

Fig.3.2 Power distribution

3.3 Radiation Pattern

It is noteworthy that the antenna acts as the array of two apertures and the distance between the apertures contribute on the radiation pattern. Radiation patterns of the antenna with different ring lengths are compared in Fig.3.3. The E-plane ($\phi = \pi/2$) and H-plane ($\phi = 0$) patterns are depicted in Fig.3.3(a) and Fig.3.3(b), respectively. The long ring antenna, i.e., c equals 0.75λ possesses the wide-beam pattern according to the too long aperture separation. This results in the decreased directivity. On the other hand the shorter ring length provide narrower beamwidth.

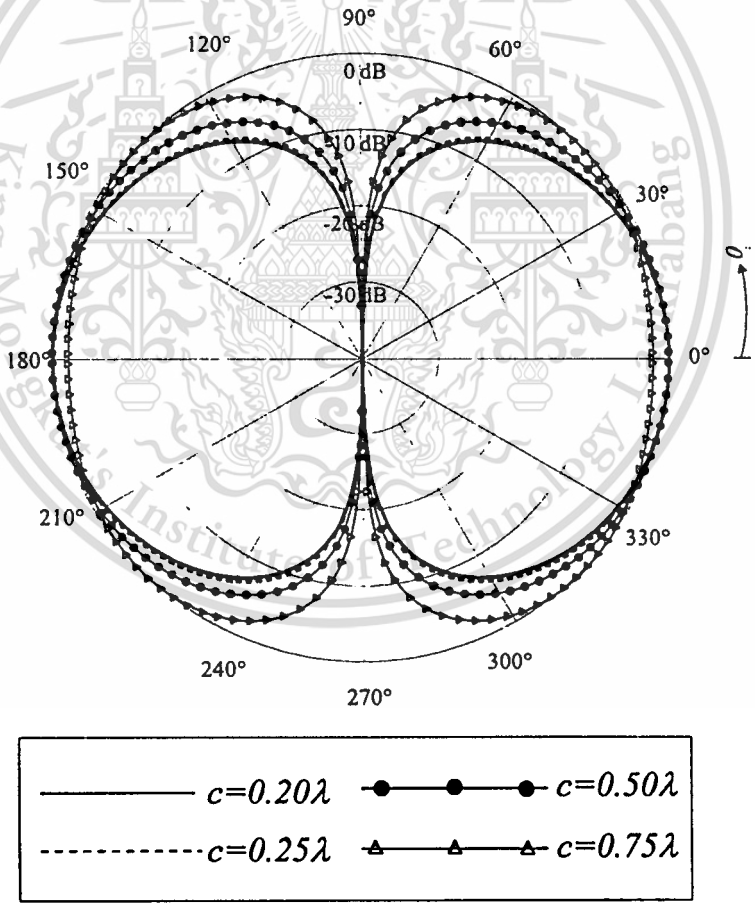

(a) E-plane

Fig.3.3 Radiation Pattern

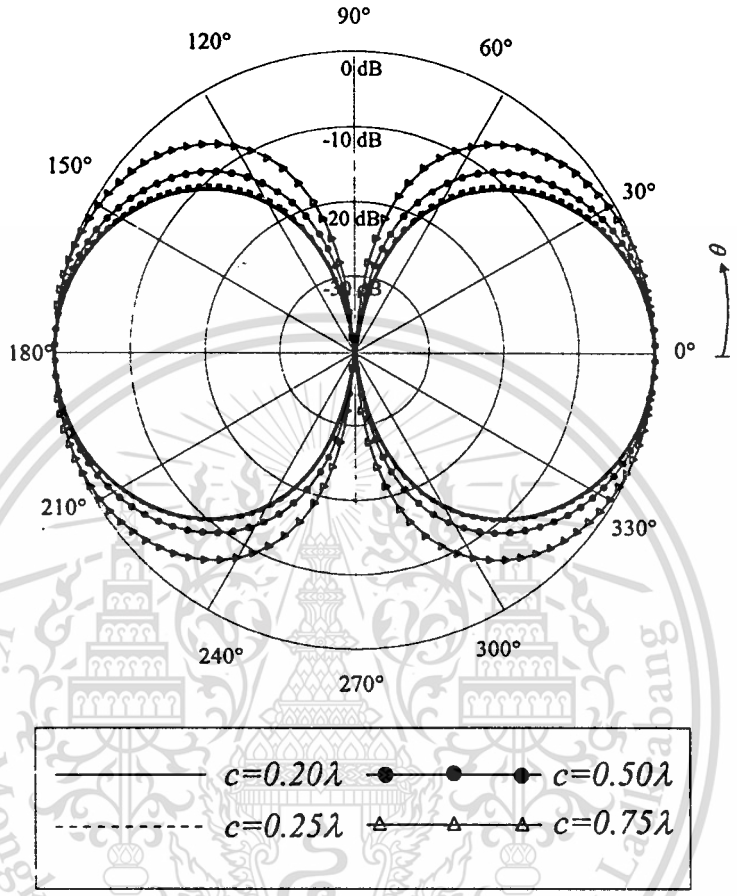

(b) H-plane

Fig.3.3 (continue)

3.4 Directivity

The optimum ring length that provides the highest directivity must be clarified. Fig.3.4 shows the directivity as a function of the ring length when l is fixed at 0.28λ, $a=0.69\lambda$ and $b=0.35\lambda$. We can observe that at the ring length of 0.25λ, the highest directivity of *6.6* dBi is achieved. Radiation patterns of the antenna when the ring length is 0.25λ that illustrates the bidirectional pattern, in E-plane and H-plane, are also posed in Fig.3.3(a) and

Fig.3.3(b), respectively. The beamwidth in the E-plane and H-plane are *80* degree and *56* degree, respectively. From this investigation, it is realized that we have to choose the ring length of 0.25λ as a design parameter.

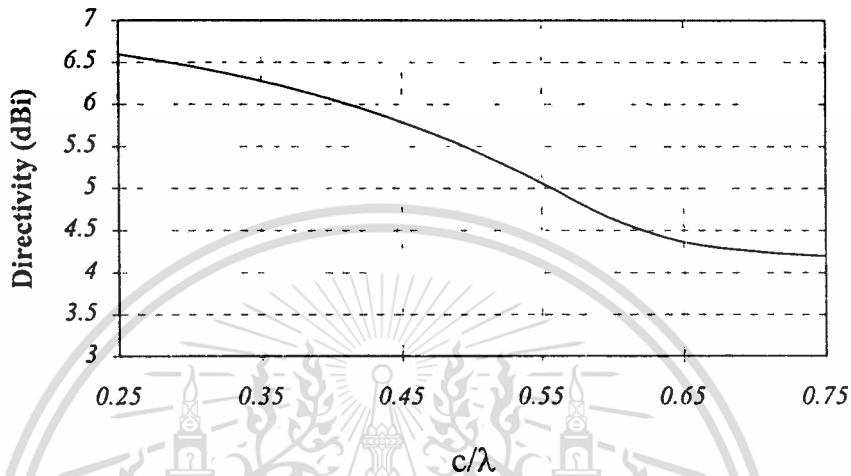

Fig.3.4 Directivity versus c/λ

3.5 Input Impedance and VSWR

To investigate impedance characteristic of this antenna, the ring dimension was fixed at the one which provides the highest directivity, i.e., a equals 0.69λ, b equals 0.35λ and c equals 0.25λ. Then the input impedance was calculated by using (2.28)-(2.30) and plotted for various probe lengths on the graph in Fig.3.5(a). When the probe length is short, l equals 0.2λ, for instance, the antenna acts has impedance with low resistance and inductive reactance. The longer the probe length, the higher the resistance and reactance. It is noted that, in Fig.3.5(b), the lowest VSWR takes place at the probe length of 0.28λ. Therefore, this length is employed as a design parameter.

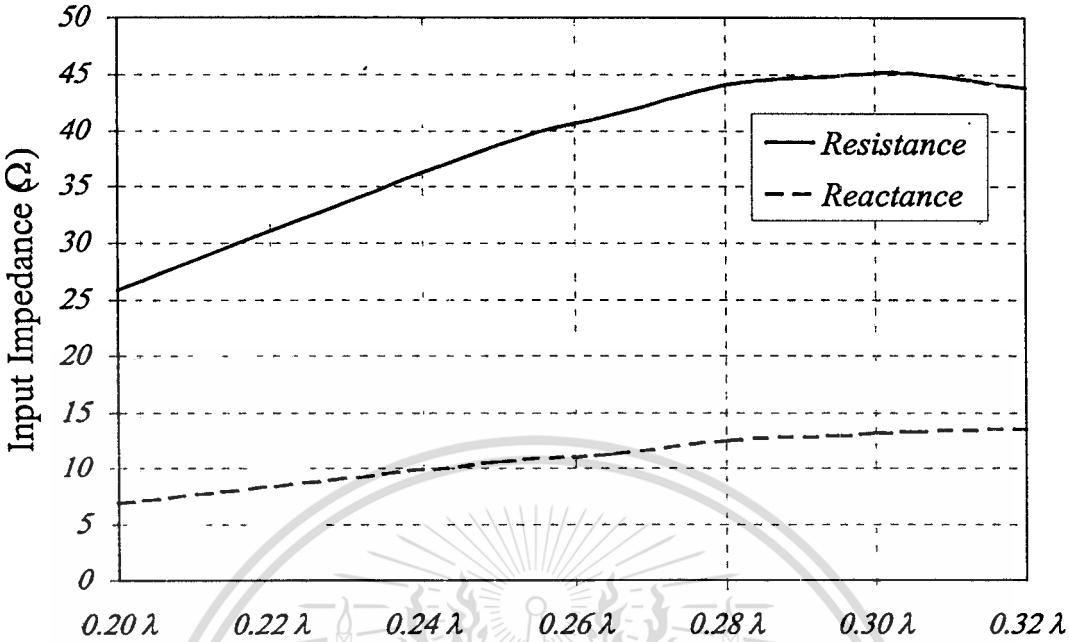

(a) Input impedance

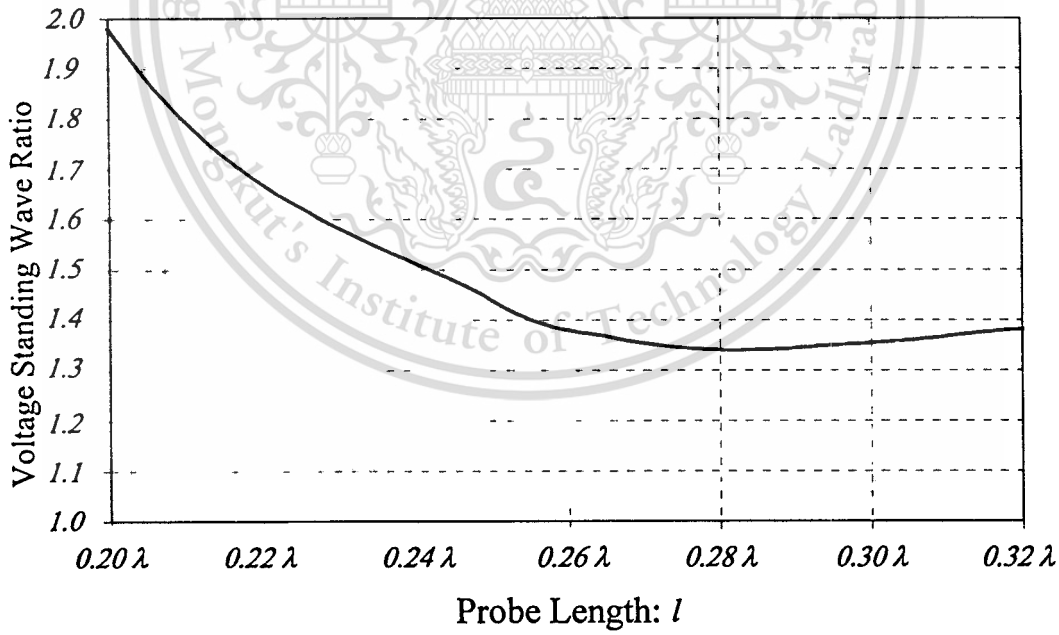

(b) Voltage Standing Wave Ratio

Fig.3.5 Input impedance and Voltage Standing Wave Ratio

3.6 Conclusion

This chapter shows numerical results of characteristics of a bidirectional antenna using a probe excited rectangular ring. The ring length must be appropriately chosen to let only a single mode appear at the apertures. It is equal to 0.25λ. Radiation patterns of the antenna having too long ring length are wide beams whereas that of the 0.25λ long possesses a narrowest single beam. It was found that as the ring length is varied, the maximum directivity of *6.6* dBi could be achieved when the ring length is equal to 0.25λ. This antenna possesses an impedance which its resistance and inductive reactance increase as the probe length is increased. The probe length of 0.28λ provides the lowest VSWR.

Chapter 4

Design of a Bidirectional Antenna Using a Probe Excited Rectangular Ring

4.1 Introduction

In this chapter the design of a bidirectional antenna using a probe excited rectangular ring are described. Prototype of bidirectional antenna is fabricated according to appropriate antenna parameters to obtain maximum directivity and matched impedance. Characteristics of the antennas are measured and compared with theoretical results.

4.2 Design Procedure

Design criteria have already been presented in Chapter 4. The parameters are appropriately selected so that maximum directivity and matched impedance can be obtained. In addition, a smallest dimension is restricted. To carry out this requirement, analytical results as illustrated in chapter 3 must be obtained. The width and the height of a ring are firstly chosen to let the dominant wave propagate in this ring. It can be made from either standard waveguide or the rectangular tube available in the market. Then the ring length that attenuates all the higher modes will be calculated by calculating aperture field or radiated field as described in chapter 3. One of the appropriate dimensions we obtained by the procedure described above is that $a=0.69\lambda$, $b=0.35\lambda$ and $c=0.25\lambda$. (For the ring of the other size, calculation must be done to obtain the appropriate length.) Once the ring dimension is obtained, the probe is designed by choosing its length at 0.28λ. It should be pointed that this antenna can be easily designed.

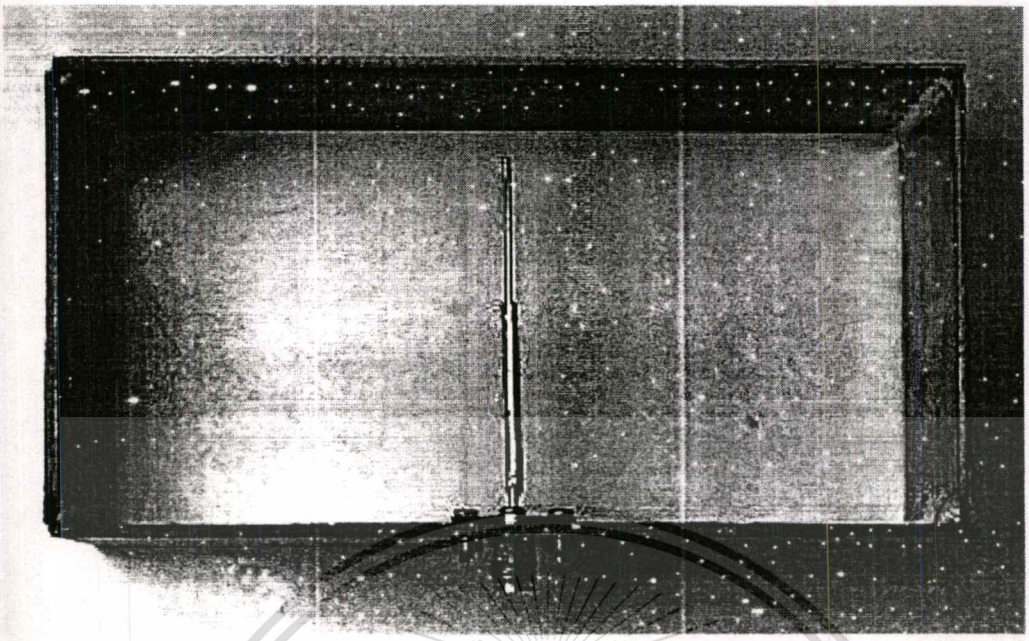

Fig.4.1 Photograph of the fabricated antenna

4.3 Experimental Results

To verify the theoretical results, a probe excited rectangular ring was fabricated to operate at the frequency of *1.9* GHz. The dimensions are as follows: *a* equals *10.92* cm, *b* equals *5.46* cm, *c* equals *3.93* cm and *l* equals *4.41* cm. The probe diameter is *1* mm. The fabricated antenna is shown in Fig.4.1. The radiation patterns were measured and plotted on the same graph of the calculated results in Fig.4.2 (a) and (b). It is obvious that the beamwidth is almost the same in E-plane at which this pattern is similar to the elevational pattern of the probe exhibited as the monopole antenna. On the other hand, the beamwidth of the pattern in H-plane of the measured results is wider than that of the predicted one. The reason is the notable effects of the ring to the radiation pattern of the probe. Since the prediction was done by approximating the total radiated fields of the antenna with the combination of the pattern from individual aperture disregarding the mutual coupling and edge effect, the predicted results exhibit narrower beamwidth than the experimental ones. However, nulls of the measured results are shallower than the prediction

counterparts due to the neglecting of edge effect and mutual coupling between the two apertures. When this antenna is investigated by using Numerical Electromagnetic Code (NEC2) based on Method of Moment at which the mutual coupling is taken into account, the pattern is similar to the measured one. Some errors take place at the null positions. This might be due to the edge effect. The detail of this matter is left for further study.

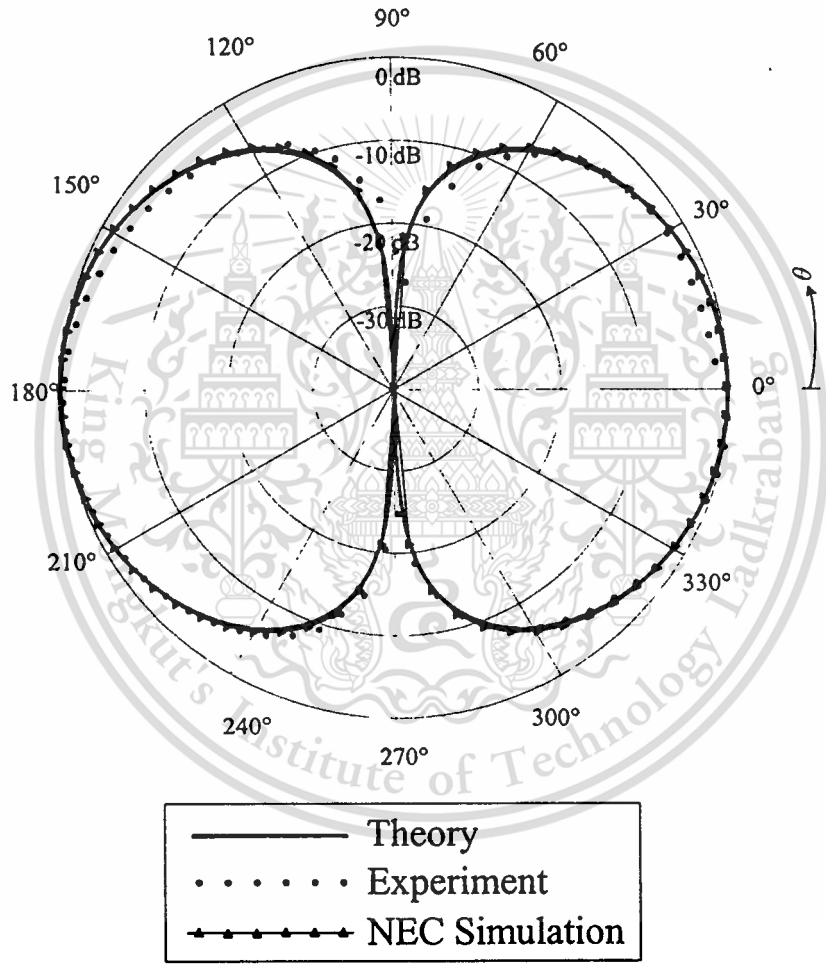

(a) E- plane

Fig.4.2 Comparison of calculated and measured radiation patterns

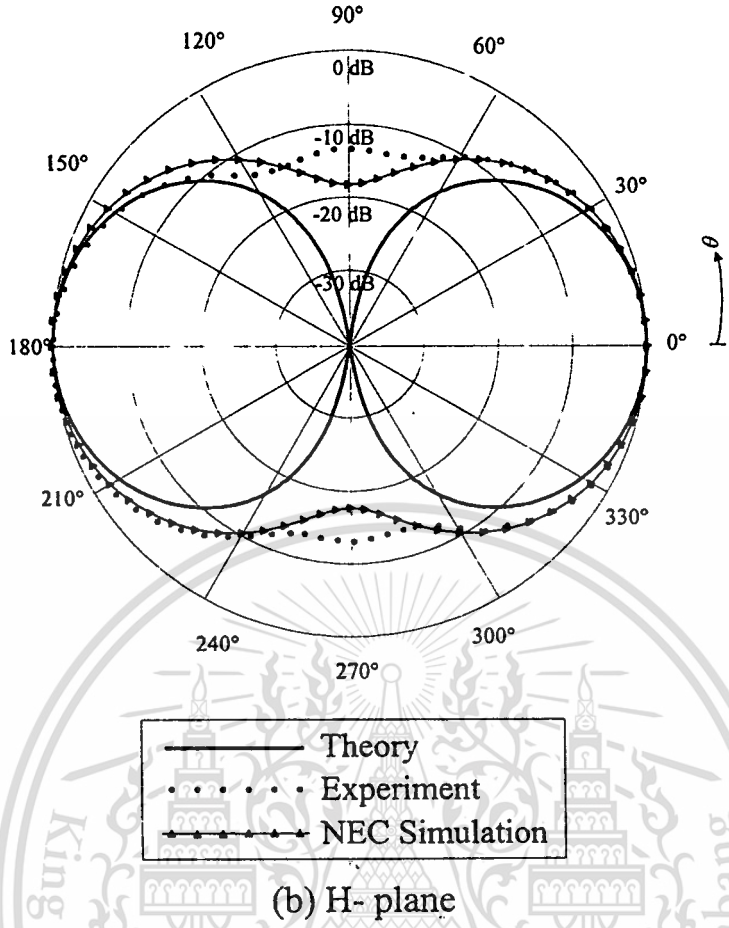

(b) H- plane

Fig.4.2 (continue)

For the impedance characteristics, the antenna was measured by using a HP8720C Network Analyzer and compared with theoretical results with TE_{10} mode consideration as illustrated in Fig. 4.3 (a). We can realize that the measured impedance is more sensitive to the frequency variation than the calculated results according to a single mode transformation of aperture admittance in calculation. However, both of the results show the same trend that we can be confident that this proposed principle is reliable. Comparison of VSWR versus frequency with the measured counterpart is depicted in Fig. 4.3 (b). It is obvious that the experimental results are slightly higher than the theoretical ones at the frequencies higher than the designed frequency. The bandwidth which VSWR less than *1.5* is *10%*.

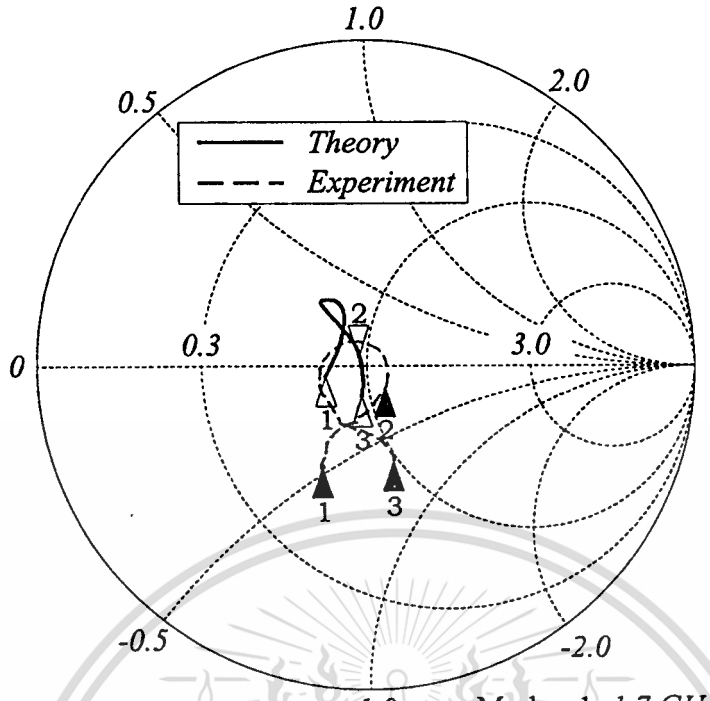

(a) input impedance

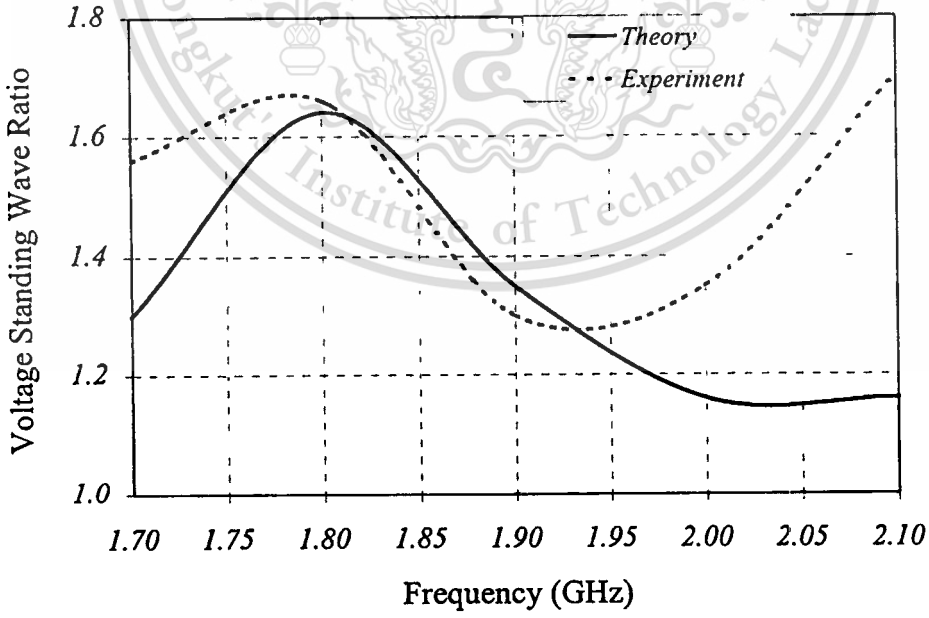

(b) VSWR

Fig.4.3 Comparison of calculated and measured input impedance and VSWR.

4.4 Conclusion

In this chapter the design of a bidirectional antenna using a probe excited rectangular ring and its procedure were discussed. It is found that we can easily design the antenna by selecting appropriate dimension of the ring and the probe. Prototype of a bidirectional antenna using a probe excited rectangular ring was fabricated. Characteristics of radiation pattern, input impedance and VSWR are measured in order to compare with theoretical results. From those results, it is clear that both of them are in good agreement, and we can see that the fabrication cost is very low since this antenna consists of only a ring and a probe. Experimental results reveal that this antenna provides a bidirectional pattern with gain of *4.5* dBi over the bandwidth of *10%*.

Chapter 5

Characteristics of a Bidirectional Antenna Using a Probe Excited Circular Ring

5.1 Introduction

Although the rectangular structure is simple for modeling, practically it is found that the circular structure is more interesting. It can be mass-produced conveniently. Hence, it is of interest to investigate a bidirectional antenna using a probe excited circular ring. In this chapter, a bidirectional antenna using a probe excited circular ring, which is simple, cost-effective and easy to fabricate, are proposed and analyzed. Aperture fields, radiation fields and directivity of the antenna are computed, and their results are discussed.

5.2 Field in a Circular Ring

A bidirectional antenna using a probe excited circular ring consists of a linear electric probe of length l protruded from a coaxial transmission line into a circular ring. The ring radius and width are a and d, respectively. The probe is oriented along the y axis as shown in Fig.5.1.

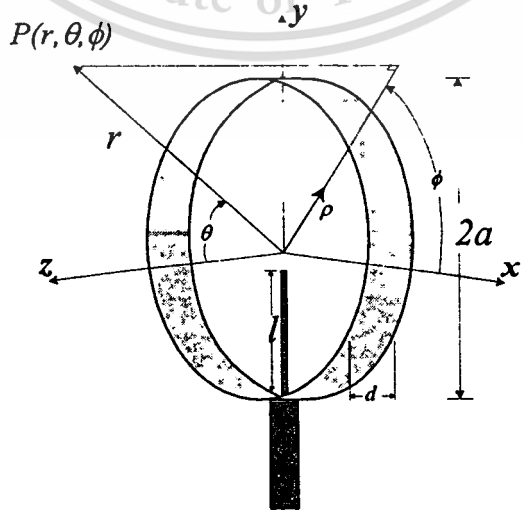

Fig.5.1 A bidirectional antenna using a probe excited circular ring

Let us consider the ring as a part of circular waveguide which electromagnetic fields propagate in both z and $-z$ directions and they radiate from the apertures at the ends of the ring. These aperture fields correspond to the composite field consisting of various modes accommodating in the waveguide. Since the ring width and radius are desired to be as small as possible, although we choose the smallest radius that cutoff all the higher modes but dominant mode TE_{11}, the field near the probe is still consisting of composite modes. Generally, the higher modes are evanescent and their amplitudes are decreased rapidly as the distance from the probe is increased. The distance is chosen such that the amplitudes of the higher modes are negligible at the apertures. Hence, the apertures radiate the fields according to only the dominant mode. To let only the dominant mode accommodated in the ring, the radius is chosen such that the lowest cut off frequency is the dominant mode TE_{11}. The adjacent mode TE_{21} is cutoff. Therefore [14]-[16], [17]

$$0.293\lambda < a < 0.486\lambda, \tag{5.1}$$

where λ is the wavelength at the operating frequency.

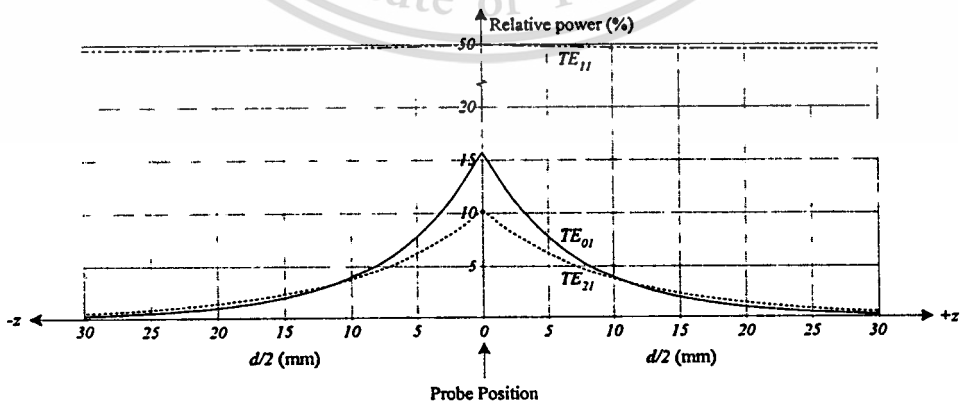

Fig.5.2 Relative amplitude of the power distribution for the three lowest modes of the ring (round copper waveguide of radius *4.75* cm with the operating frequency of *1.9065* GHz)

Since the structure of the antenna is a part of the circular waveguide, in this circumstance the radius and the width of the ring can be either standard waveguide or waveguide available in the market that is operating in a dominant TE_{11} mode. Let us consider Fig. 5.1, the electric probe inside the waveguide is parallel to the radius of the ring, therefore the TE_{mn} mode is excited. In the vicinity of the probe the field is very complex, for a given operating frequency the possible significant modes are TE_{11}, TE_{21}, TE_{01} and etc. As the waves travel along the waveguide toward the two open apertures, they will be attenuated. The attenuation constant, α_{11} for TE_{11} wave in dB/m is

$$\alpha_{11} = \frac{R_s}{a\eta} \frac{8.686}{\sqrt{1-\left(\frac{\lambda}{\lambda_{c11}}\right)^2}} \left[\left(\frac{\lambda}{\lambda_{c11}}\right)^2 + 0.420\right] \tag{5.2}$$

where λ_{c11} denotes the cutoff wavelength of the TE_{11} mode which equals $3.412a$, η is the intrinsic impedance of the medium and R_s is the frequency-dependent characteristic resistance of the metal walls. If the free-space wavelength is greater than the critical wavelength of any particular mode, the evanescent waves, TE_{21} and TE_{01}, are then attenuated with distance according to the factor $e^{-\alpha z}$. The attenuation constant α_{21} for TE_{21} wave in dB/m is

$$\alpha_{21} = \frac{17.372\pi}{\lambda_{c21}} \sqrt{1-\left(\frac{\lambda_{c21}}{\lambda}\right)^2} \tag{5.3}$$

and for TE_{01} mode

$$\alpha_{01} = \frac{17.372\pi}{\lambda_{c01}} \sqrt{1 - \left(\frac{\lambda_{c01}}{\lambda}\right)^2} \tag{5.4}$$

where λ_{c21} and λ_{c01} are the cutoff wavelength of TE_{21} and TE_{01} modes, respectively, which $\lambda_{c21} = 2.057a$ and $\lambda_{c01} = 1.640a$. The relative amplitude of the power distribution for the three lowest modes of the ring at the operating frequency of *1.9065* GHz from (5.2) through (5.4) can be illustrated in Fig.5.2. The power flow in the TE_{mn} mode can be expressed in the form $P = |A|^2 \omega\mu\beta A_{mn}$ in which A_{mn} depends only on the mode indics. The numerical results are given in table I.

Table 5.1 The coefficients A_{mn}

$A_{mn} \times 10^{-3}$			
n \ m	1	2	3
1	17.4	55.3	11.4
2	2.87	3.19	1.56
3	0.349	0.794	0.492

It is apparent that the total maximum normalized amplitude of TE_{11} mode is *100%,* and for TE_{21} and TE_{01} counterparts, the amplitudes are *20.61%* and *31.46%,* respectively [18]. However, since the power is equally divided to propagate in both *z* and *-z* directions the amplitude is shown at *50%, 10.31%* and *15.73%,* respectively. The distance beyond the cross-over point between the power curve of TE_{21} and TE_{01} will be selected as the optimum width because at this point the power of the strongest higher mode, TE_{21} is attenuated by *5.32* dB or it is reduced to negligible level less than *10%* of the power of the dominant TE_{11} mode. The other higher order mode

power, including TE_{01} mode, is less than that of the TE_{21} one. The following calculation is shown as a guideline to design for any other ring radii. For example, if $a = 4.7506$ cm, $f = 1.9065$ GHz, by using (5.3) the nominal attenuation constant of TE_{21} mode is *0.4378* dB/mm. It requires that the distance of *d/2* equals *12.1517* mm to reduce the power of the TE_{21} mode to *3.028%* or attenuated by *5.32* dB. In the same fashion, by using (5.2) the attenuation constant of TE_{11} mode (α_{11}) equals *0.0000169* dB/mm. Hence at *d/2 = 12.1517* mm, the power of the TE_{11} mode becomes *49.9976%.* The ratio of the TE_{11} mode power to TE_{21} mode power is equal to *16.5117.* Therefore, the power of the TE_{11} mode is more *16* times stronger than the power of the TE_{21} mode. This situation results that the field distribution at the apertures will be the dominant TE_{11} mode while the power of the other higher order modes can be sufficiently negligible. To confirm the level of the other higher modes, the attenuation constant of TE_{01} mode (α_{01}) is also calculated and found to be *0.6087* dB/mm. Therefore, at the distance of *12.1517* mm from the probe, the power of the TE_{01} mode becomes *2.8645%.* The ratio of the TE_{11} mode power to TE_{01} mode power is equal to *17.4524* at which is negligently small. It is pointed that in the design, the ring width (*d*) can be easily determined by calculating the distance from the probe that the attenuation constant of TE_{21} mode becomes *5.32* dB because the power of TE_{21} mode is the strongest higher mode.

5.3 Aperture Field

It was described that we have to select the ring radius so that it can support the dominant wave to propagate in the ring while attenuate all the higher modes. Therefore, there will be only the dominant wave at the apertures. It can be expressed as [11]

$$E_\rho = \frac{2\sin\phi}{\rho} J_1\left(1.84\frac{\rho}{a}\right) \tag{5.5a}$$

$$E_\phi = \frac{2a\cos\phi}{1.84} \frac{dJ_1\left(1.84\frac{\rho}{a}\right)}{d\rho} \tag{5.5b}$$

where J_1 is the Bessel function of the first kind and order 1, *1.84* is the first zero (n=1) of the derivative of the Bessel function of the first kind of order one (m=1) and ρ is the cylindrical radial coordinate shown in Fig.5.1. In rectangular coordinates the expression for the field distribution are given by

$$E_x = E_\rho \cos\phi - E_\phi \sin\phi \tag{5.6a}$$

$$E_y = E_\rho \sin\phi + E_\phi \cos\phi \tag{5.6b}$$

By substituting (5.5a) and (5.5b) into (5.6a) and (5.6b) and with some algebraic manipulations, it is found that

$$E_x = J_2\left(1.84\frac{\rho}{a}\right)\sin 2\phi \tag{5.7a}$$

$$E_y = J_0\left(1.84\frac{\rho}{a}\right) - J_2\left(1.84\frac{\rho}{a}\right)\cos 2\phi \tag{5.7b}$$

where J_2 and J_0 are the Bessel function of the first kind of the second and zeroth order.

The expressions in (5.7a) and (5.7b) are the aperture distribution of a bidirectional antenna using a probe excited circular ring.

5.4 Radiated Field

Radiation characteristic of the antenna is reported in this section. Radiation fields of the antenna from the two circular apertures are calculated by superposing the fields that radiated from each aperture. The far-field observation of these two apertures is shown in Fig.5.3.

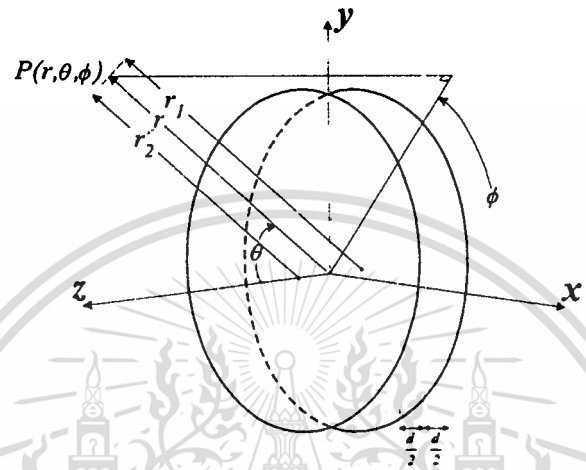

Fig.5.3 Far-field observation of the two circular apertures

If mutual coupling between the two apertures and the edge effect at the apertures are neglected; therefore, the total radiated field is considered to be the superposition of the field from each aperture. Additionally, since the radiated fields from the two apertures have the same phase but in opposite directions; hence, when they are combined, the resultant electric field due to dominant TE_{11} mode, can be expressed as [14]-[15]

$$E_\theta = A_{11} a^2 \sin\phi \frac{J_1(\chi_{11})}{\chi_{11}} \frac{J_1(ka\sin\theta)}{ka\sin\theta} \sin\left(\frac{1}{2}kd\cos\theta\right) \tag{5.8}$$

and

$$E_\phi = A_{11} a^2 \cos\theta\cos\phi \frac{\chi_{11} J_1(\chi_{11})}{\chi_{11}^2 - (ka\sin\theta)^2} J_1'(ka\sin\theta) \cdot \sin\left(\frac{1}{2}kd\cos\theta\right) \tag{5.9}$$

where A_{11} denotes the relative amplitude of the TE_{11} mode field, $J_1(*)$ is the ordinary Bessel function of the first kind of order *1*, k is the wave number of free space and the prime is the derivative with respect to the argument $(ka\sin\theta)$. These field expressions are employed to investigate the radiation patterns and directivity of the antenna when the width is long enough. They cannot be applied to the shorter ring case.

From the radiated field mentioned above, the radiation pattern of a bidirectional antenna using a probe excited circular ring for the three cases are illustrated. The operating frequency is *1906.55* MHz. Firstly, the generally available waveguide of the radius *4.75* cm (0.3019λ) is utilized as the ring. Secondly, the standard waveguide WC451 of the radius *5.73* cm (0.3641λ) is used. Lastly, the standard waveguide WC528 of the radius *6.71* cm (0.462λ) is demonstrated. The radiation patterns of these three illustrations are plotted in the two principal planes; E-plane (E_θ for constant $\phi=\pi/2$) and H-plane (E_ϕ for constant $\phi=0$), as shown in Fig. 5.4 through Fig.5.6, respectively. The difference of the ring width of 0.3λ is used throughout the calculation of three cases. For all of the three cases, it is obvious that when the ring width is longer than the optimum length, i.e., $d=0.15\lambda$ (for available waveguide of the radius 0.3019λ), $d=0.22\lambda$ (for WC451 waveguide) and $d=0.35\lambda$ (for WC528 waveguide), which is shown by the solid line, the broader beam can be explicitly observed. The bidirectional patterns are confidently achieved at the optimum ring width. When the ring width is greater than around 0.7λ, the split beam is gradually occurred. It is noted that this optimum length is shortest length that the ring possesses only the dominant mode which the pattern can be characterized by using (5.8) and (5.9). If the ring width is shorter than the optimum length, equation (5.8) and (5.9) are not applicable.

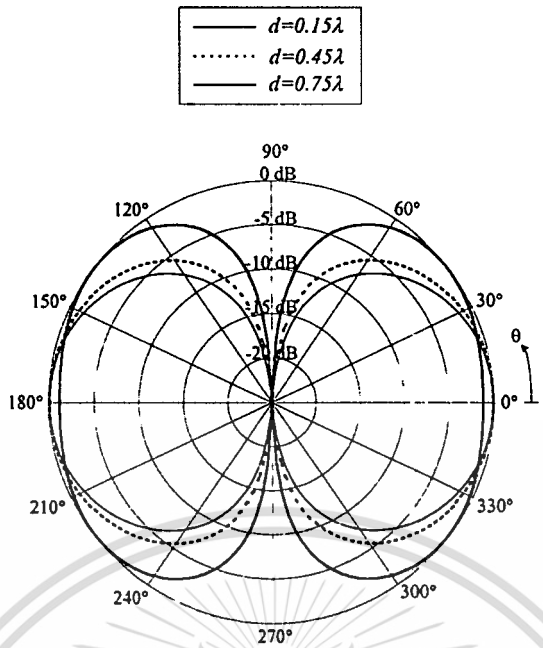

(a) E-Plane

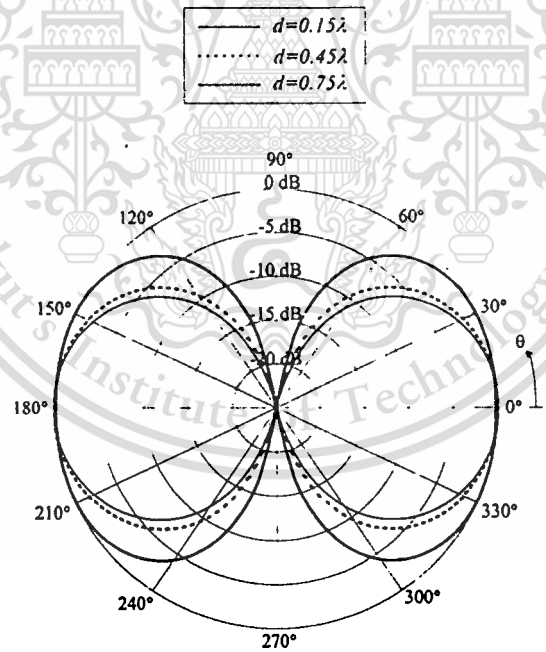

(b) H-Plane

Fig.5.4 Radiation patterns of the antenna utilizing an available waveguide of radius 0.3019λ for various ring widths

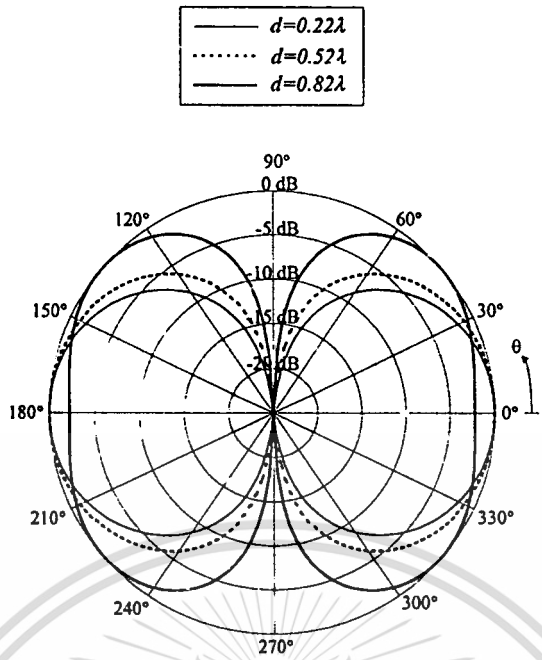

(a) E-Plane

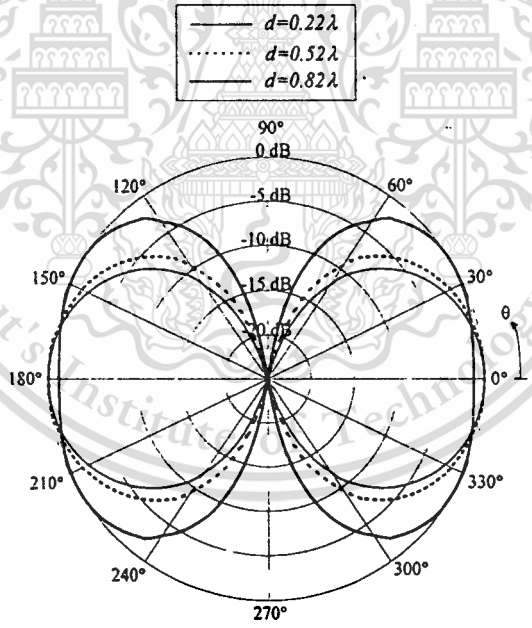

(b) H-Plane

Fig.5.5 Radiation patterns of the antenna utilizing the standard waveguide WC451 *(a=0.3641λ)* for various ring widths

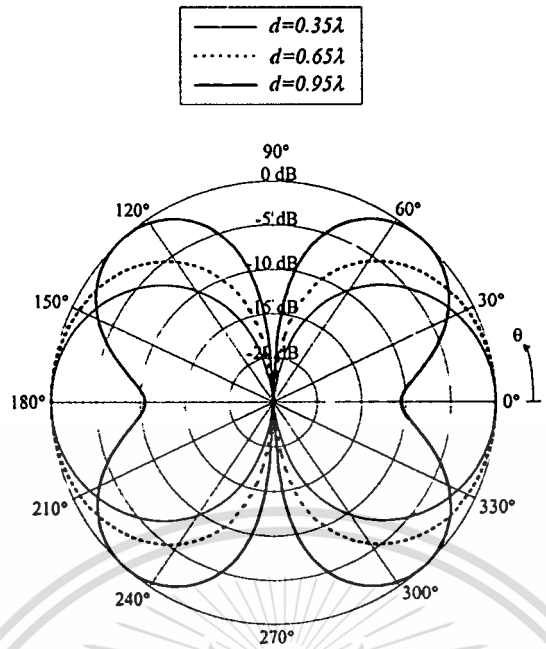

(a) E-Plane

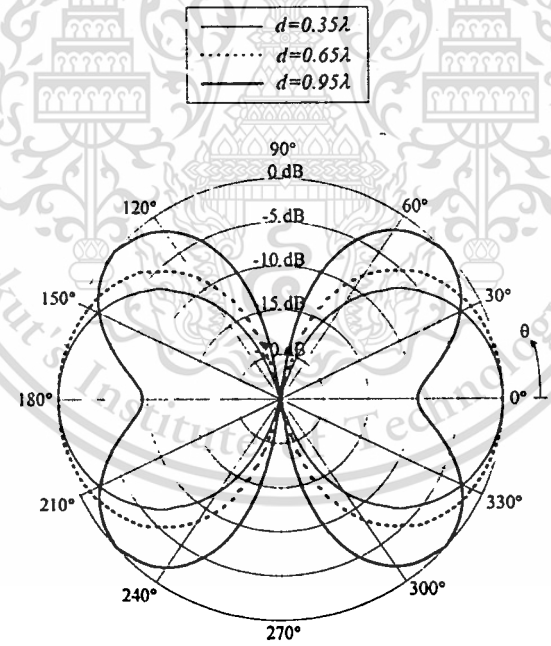

(b) H-Plane

Fig.5.6 Radiation patterns of the antenna utilizing the standard waveguide WC528 ($a = 0.4262\lambda$) for various ring widths

5.5 Directivity

Directivity of a bidirectional antenna using a probe excited circular ring is calculated for various ring widths and shown in Fig.5.7. It is obvious that the ring width of the antenna that provides the highest directivity is obtained when $d=0.15\lambda$ (for available waveguide of the radius 0.3019λ), $d=0.22\lambda$ (for WC451 waveguide) and $d=0.35\lambda$ (for WC528 waveguide). Since results for smaller d not available, optimum d is not determined in this section. The maximum directivity for these three cases is more than about 7 dBi. It is seen that for the same ring width such as $d=0.49\lambda$, the larger waveguide radius (WC528) gives the higher directivity than the smaller waveguide radii (WC451 and 0.3109λ waveguide). In addition, for the same ring radius, the longer ring width, the lower directivity.

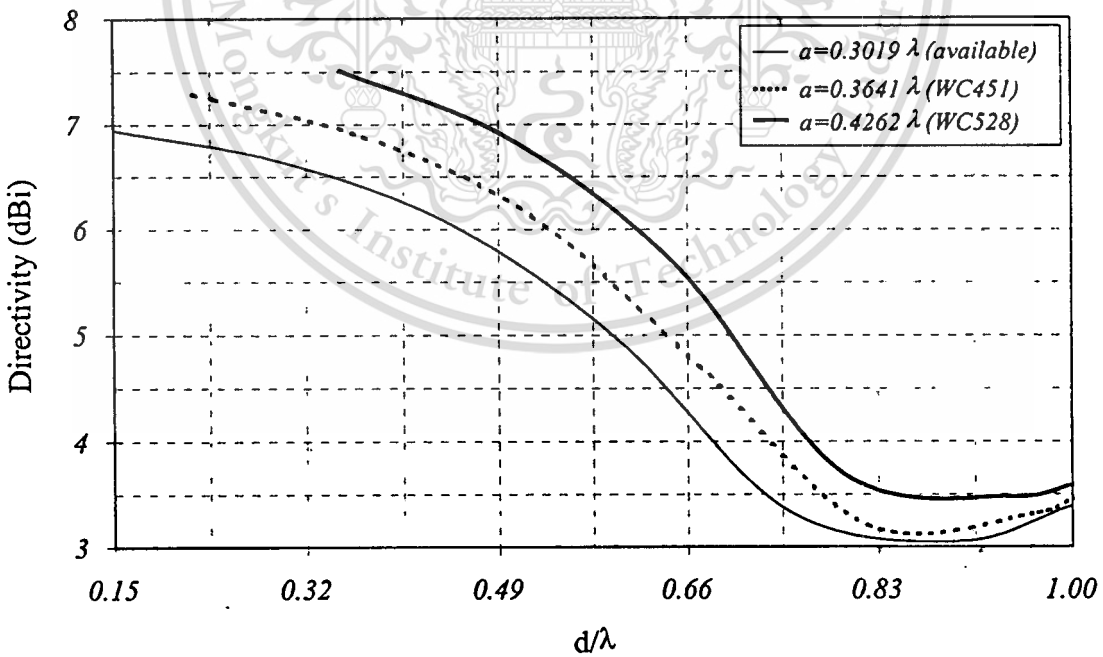

Fig.5.7 Directivity of the antenna utilizing the three waveguide radii versus the ring width

5.6 Conclusion

A bidirectional antenna using a probe excited circular ring has the same principle as that of the rectangular one. However, the calculation of the ring width can be achieved, by using attenuation constant of wave at various modes, instead of aperture field calculation. This results in a simple task. Numerical results clarified that the short ring width provides a split beam and low directivity. On the other hand, the too long ring width makes the too long aperture separation to result in the low directivity as well. Therefore, an appropriate ring width must be chosen.

Chapter 6

Design of a Bidirectional Antenna Using a Probe Excited Circular Ring

6.1 Introduction

This chapter describes the design of a bidirectional antenna using a probe excited circular ring and the experimental results as its estimation. The design curve is firstly constructed from the principle introduced in chapter 5. Then, the antenna is designed at the operating frequency of *1.9605* GHz. Prototypes of the bidirectional antennas are fabricated. Characteristics of the antenna such as radiation patterns, impedance and gain are measured. Experimental results are compared with theoretical results in figures. The communication range estimation is also done.

6.2 Design Procedure

According to the field expression in (5.8) to (5.9), the characteristic curve of the antenna can be illustrated for the usable ring radius. It is represented in Fig.6.1.

From Fig.6.1(a), the optimum ring width providing the maximum directivity for specified ring radius is illustrated by the solid line.

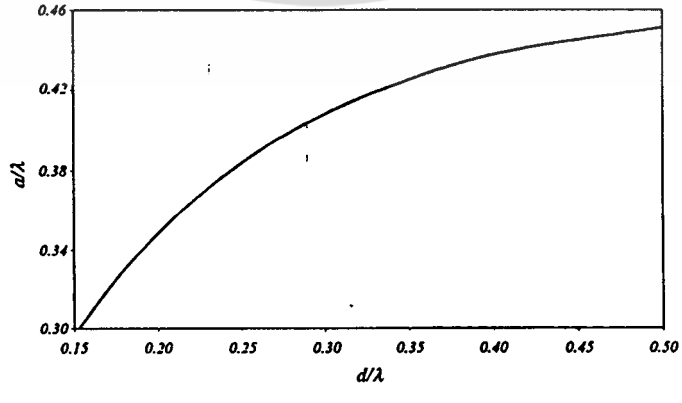

(a) design curve

Fig.6.1 Antenna design criterion

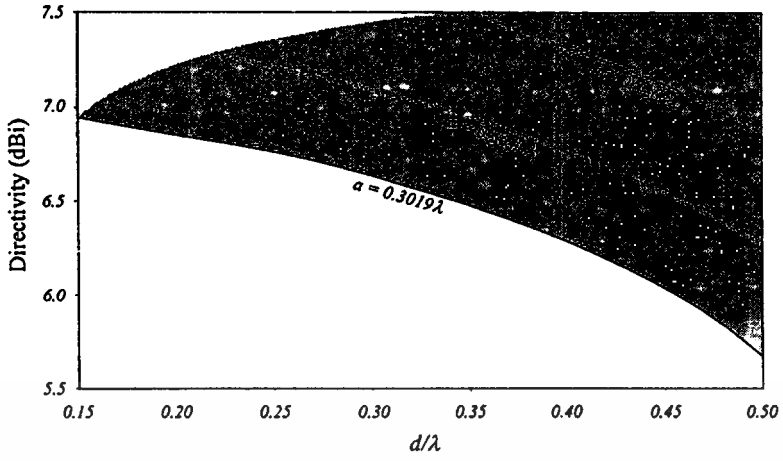

(b) directivity versus the ring width

Fig.6.1 (continue)

This graph is very useful as the guideline for the antenna design. For instance, there is a specific width for a specified ring radius that the antenna radiates a single mode and provides the maximum directivity i.e., when a equals 0.36λ the ring width will be 0.21λ. For other ring radii in the range of (5.1), this graph is also very convenient to find the optimum ring width. However, it is noticed that when the ring radius is further increased to more than 0.40λ, the optimum ring width providing the maximum directivity is drastically increased. This situation results the antenna structure to be very large and difficult to install for practical use. In Fig.6.1(b), the directivity versus the ring width for different ring radii is also shown by the shadow region. It is obvious that the directivity of the antenna is in the range of *5.5-7.5* dBi. This graph is very useful to determine the directivity for the various ring widths of the different radii. The dash line specifying three ring radii, $a = 0.4262\lambda$ (WC528 or $a = 6.7056$ cm at $f = 1.9065$ GHz), $a = 0.3641\lambda$ (WC451 or $a = 5.7277$ cm at $f = 1.9065$ GHz) waveguides and available waveguide when a equals 0.3019λ ($a = 4.7506$ cm at $f = 1.9065$ GHz) are depicted as the guideline. For any other waveguide sizes with the dimension among these three

sizes, it can be evaluated by interpolating from these dash lines. For example, if the waveguide of the radius 0.35λ is available and the directivity of *6.5* dBi is required, the ring width should be 0.44λ. Alternatively, if the ring radius of 0.40λ and the ring width of 0.37λ are chosen, the obtained directivity is *7.4* dBi. Eventually, among these three parameters (ring radius, ring width and directivity) if two parameters are first specified, the other parameter can be estimated. It is also pointed out that for the same ring width such as $d = 0.39\lambda$, the larger waveguide radius gives the higher directivity than the smaller waveguide radii. In addition, for the same ring radius, the longer the ring width, the lower the directivity. The directivity for the ring width larger than 0.50λ is also calculated and it is evident that the directivity is rapidly decreased due to the split beam from the large spacing of the two apertures. Hence, for the ring width larger than 0.50λ, this antenna is not suitable because the bidirectional pattern is not obtained.

6.3 Experimental Results

6.3.1 Radiation Pattern

According to the design criterion in (5.1) a bidirectional antenna using a probe excited circular ring is designed to operate at the frequency of *1.9065* GHz and it is fabricated. The probe length is fixed at *3.93* cm (0.25λ). In order to design the ring width of this antenna, a curve of Fig.6.1 is used. It is found that for the ring radius of *4.7506* cm (0.3019λ) the optimum ring width is 0.154λ (*2.43* cm). The radiation pattern of this antenna was measured in both E-plane and H-plane as illustrated in Figs.6.2(a) and 6.2(b), respectively. These results are compared with the approximation formulae from (5.8) and (5.9). From Fig.6.2, it is obvious that the beamwidth is almost the same in E-plane at which this pattern is

similar to the elevational pattern of the probe exhibited as the monopole antenna. On the other hand, the beamwidth of the pattern in H-plane of the measured results is wider than that of the predicted one. The reason is the notable effects of the ring to the radiation pattern of the probe. Since the prediction was done by approximating the total radiated fields of the antenna with the combination of the pattern from individual aperture disregarding the mutual coupling and edge effect, the predicted results exhibit narrower beamwidth than the experimental ones. However, nulls of the measured results are shallower than the prediction counterparts due to the neglecting of edge effect and mutual coupling between the two apertures. When this antenna is investigated by using Numerical Electromagnetic Code (NEC2) based on Method of Moment at which the mutual coupling is taken into account, the pattern is similar to the measured one. Some errors take place at the null positions. This might be due to the edge effect. The detail of this matter is left for further study.

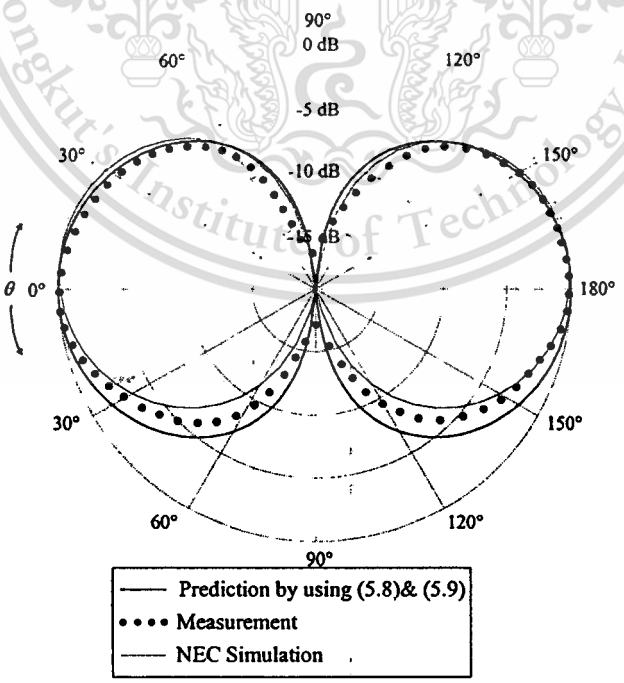

(a) E-plane

Fig.6.2 Comparison between measured and predicted patterns

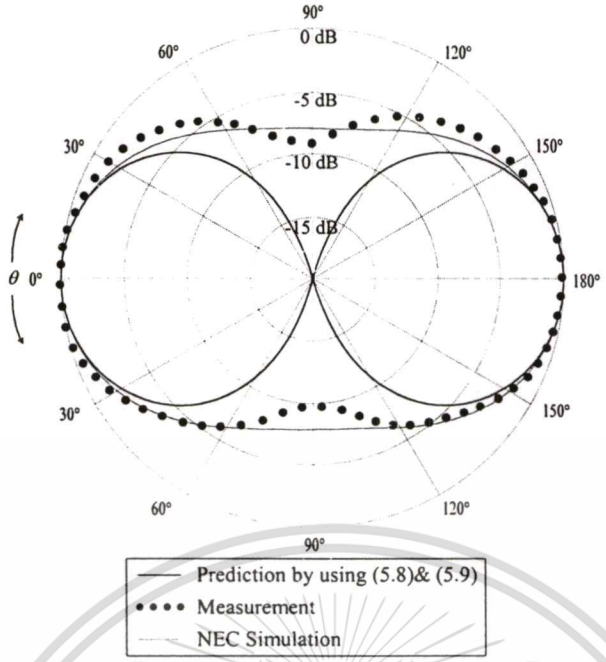

(b) H-plane

Fig.6.2 (continue)

To investigate the antenna characteristics, the antennas with three ring widths are fabricated i.e., 0.050λ, 0.154λ and 0.450λ. The photograph of these fabricated antennas is depicted in Fig.6.3.

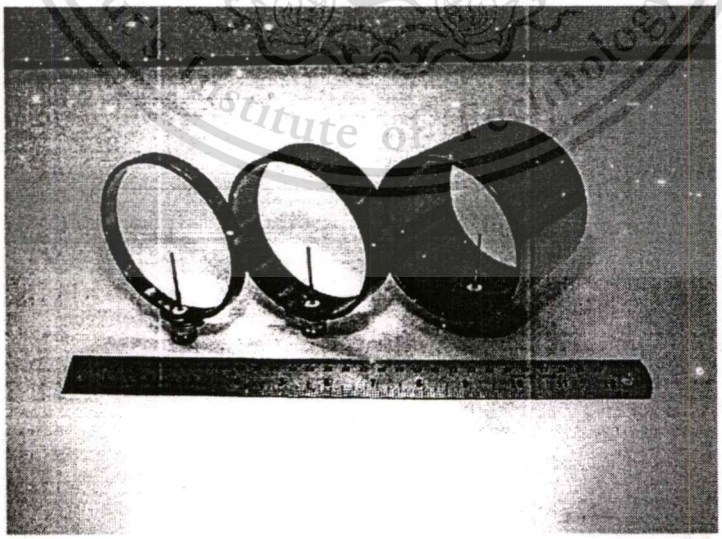

Fig.6.3 Photograph of the fabricated antenna

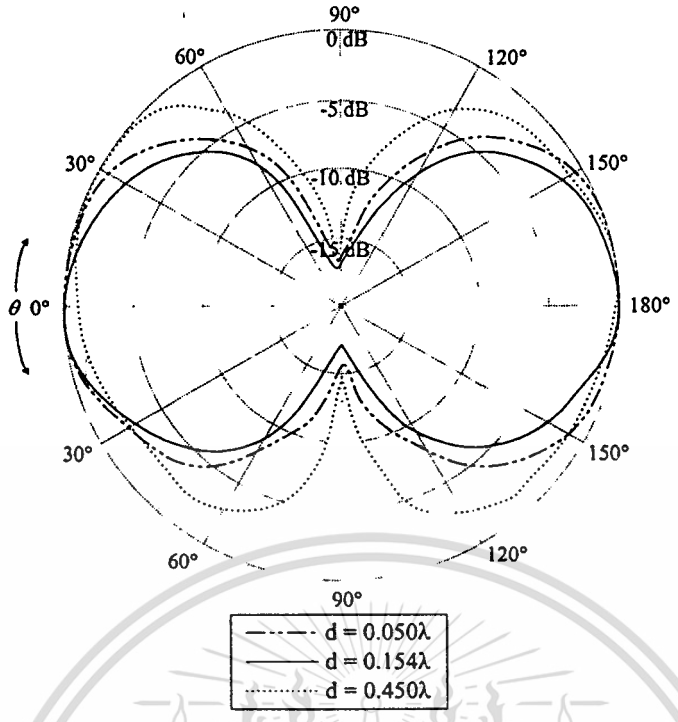

(a) E-plane

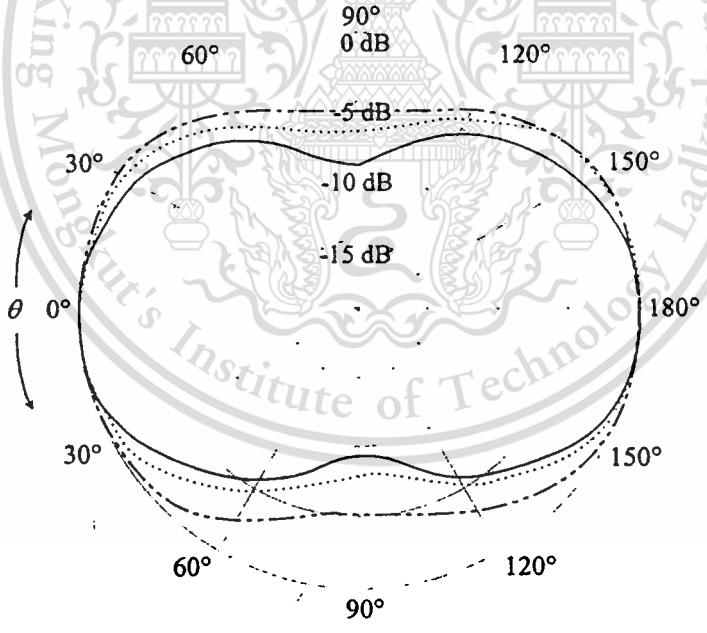

(b) H-plane

Fig.6.4 Radiation pattern of the antenna for various ring widths

Then, the antenna patterns were measured and plotted to compare with each other. The results in E-plane and H-plane are shown in Fig.6.4 (a) and 6.4(b), respectively. The pattern of the 0.050λ ring width antenna has larger beamwidth in both E and H planes since its width is too short for the higher modes to die out. Hence, the aperture fields consist of many modes. On the other hand, the beamwidth of the antenna with ring width of 0.450λ is wide due to the ring width is too long. These results confirm the validity of the design procedure. Moreover, the cross polarization pattern was measured. We found that this antenna has the cross polarization isolation of about *10* dB. It is possible to propose as a polarization diversity antenna at which is left for further study.

6.3.2 Input Impedance

The radiation characteristics described in the previous section are obtained from the design procedure that the ring radius is chosen to let only the dominant mode accommodated in the ring using (5.1). Then, the ring width is chosen from the graph in Fig.6.2. The probe length was set at 0.25λ. However, the optimum condition for matching was not clarified in the preceding section. In this section, we show the impedance characteristic of the antenna which can be simply improved by adjusting the probe length. This principle is carried out by the experiments.

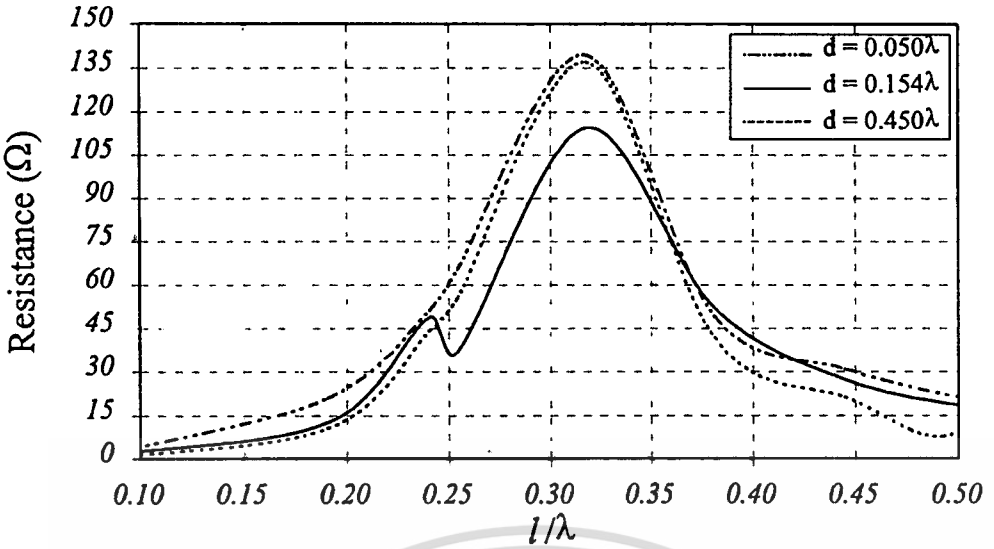

Fig.6.5 Resistance for various probe lengths

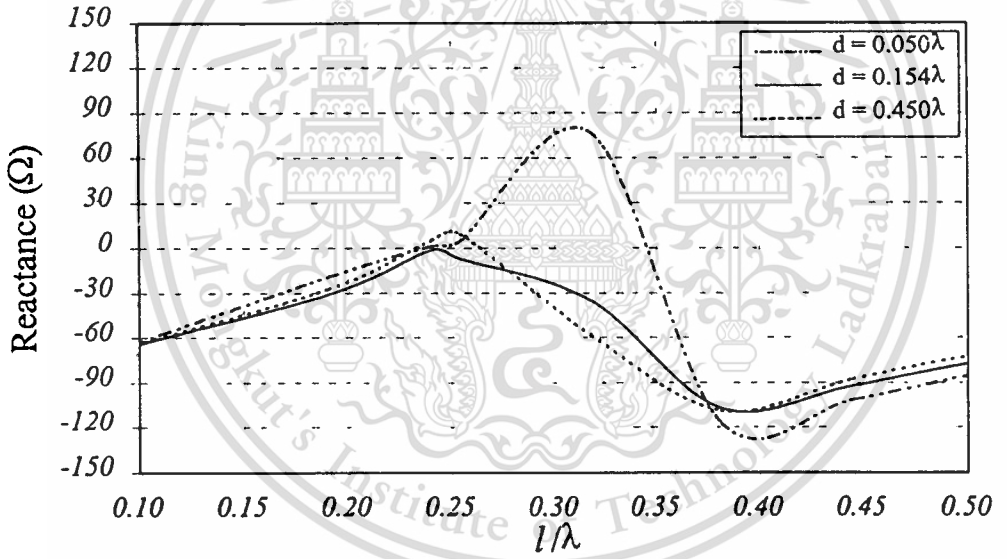

Fig.6.6 Reactance for various probe lengths

Fig.6.5 and Fig.6.6 show the measured resistance and reactance, respectively, as a function of the probe length of the three antennas. The dimension of these antennas are as follows; a equals *0.3019λ* and d equals *0.050λ*, *0.154λ* and *0.450λ*, respectively. The variations of resistance of the three antennas are almost the same manner. They

increase from small value of a few ohms at the short probe length (0.10λ) and they have the peak value when l is approximately 0.32λ. Then the resistance is smaller as the probe length is further increased. The reactance of the antenna of these three widths are in the same fashion. They are capacitive reactance of around $60\ \Omega$ when l equals 0.10λ. This reactance tends to resonate at l is approximately 0.25λ then return to capacitive reactance again as the probe length is further increased. These characteristics are nominated by monopole field. The VSWR versus the probe length is shown in Fig.6.7.

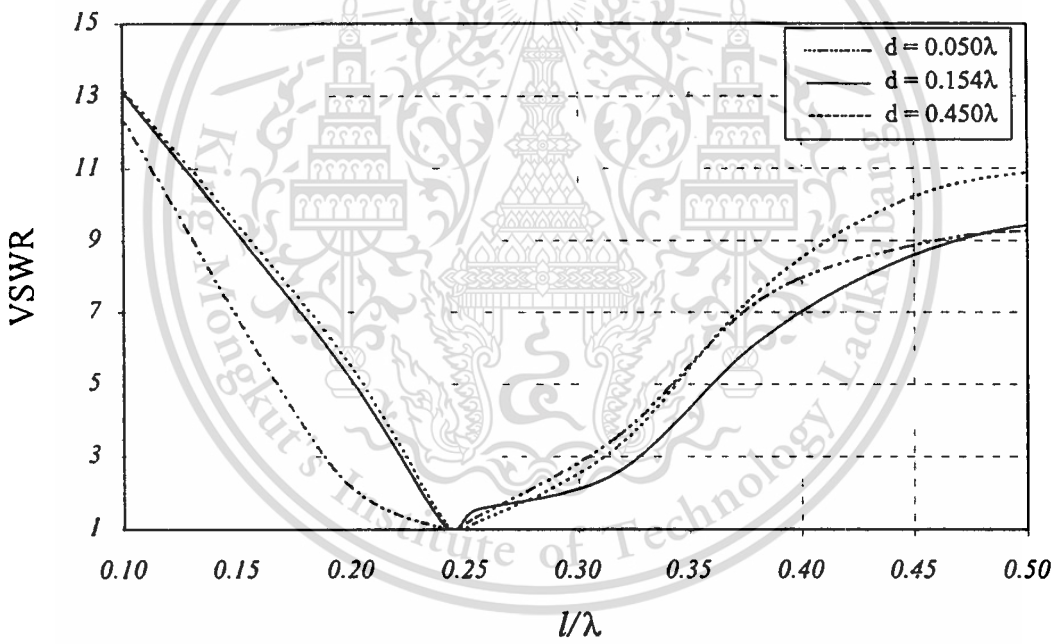

Fig.6.7 Voltage Standing Wave Ratio for various probe lengths

From Fig.6.7, it is obvious that the minimum VSWR in all cases occur when l equals 0.24λ. Therefore, this value is specified as a design parameter. According to the aforementioned that the optimum antenna parameters i.e., a equals 0.3019λ, d equals 0.154λ, and l equals 0.24λ, the antenna for this specified dimensions was fabricated. The probe diameter

of 1 mm is used. The impedance and VSWR versus the frequency of the antenna were measured as shown in Fig.6.8 and Fig.6.9, respectively. The antenna has the capacitive reactance at the frequency below and above the design frequency as shown in Fig.6.8. It is almost resonance ($Z = 50.9 - j3.5\ \Omega$) at the design frequency.

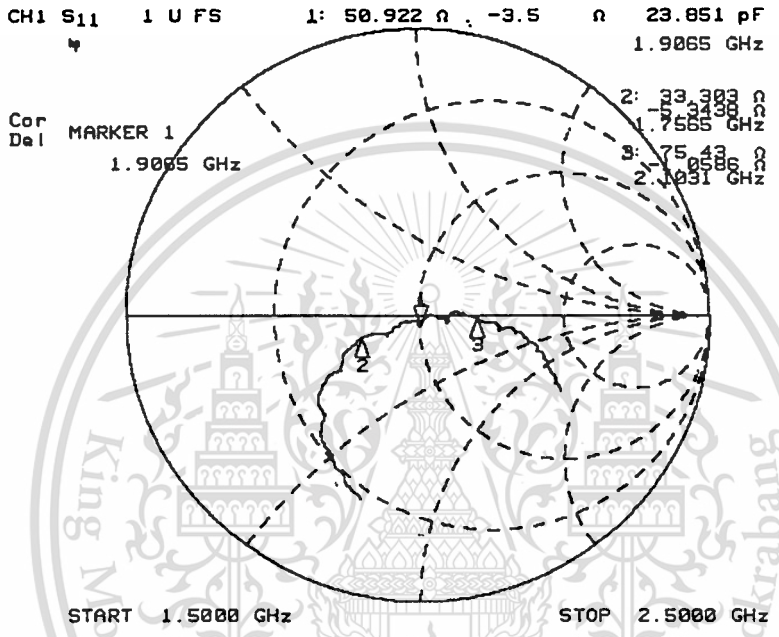

Fig.6.8 Measured impedance of the antenna

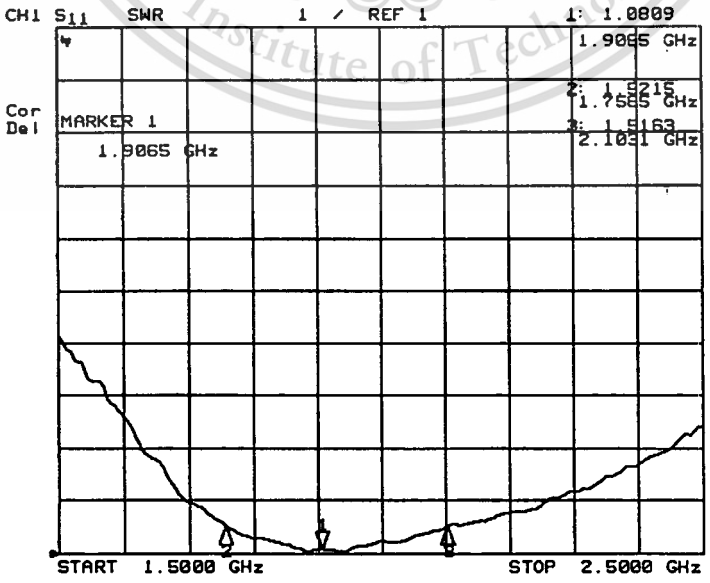

Fig.6.9 Measured standing wave ratio of the antenna

From Fig.6.9, it is relevant that the bandwidth of VSWR ≤ *1.5* is *17.8%* which is excessively wide for practical use in mobile communication system.

6.3.3 Gain

Two identical corner reflector antennas were fabricated and measured the gain using the Friis transmission equation [12]. The gain of *7.1*, *7.3* and *7.5* dBi at the frequency of *1.7000*, *1.9065* and *2.1000* GHz, respectively, were measured. By using the substituting method, the bidirectional antenna using a probe excited circular rings designed to operate at the frequency of *1.9065* GHz were measured. It is found that the designed antenna has the gain of *5.4*, *5.6* and *5.4* dBi at *1.7000*, *1.9065* and *2.1000* GHz, respectively. The results in this section verify that this antenna provides a bidirectional pattern of gain about *5.4* dBi in the bandwidth of about *17%*. We also measured the patterns in this bandwidth and found that they are not significantly changed.

6.4 Communication Range Estimation

When the antenna was installed on the roadside, its pattern will cover the road as shown in Fig.6.10. If the space is free of reflection and scattering from objects, the free space is considered. We can estimate the communication range by calculating the power received by the mobile unit when the bidirectional antenna using a probe excited circular ring is employed as a base-station antenna. In this demonstration, the operating frequency is chosen to be *1.9065* GHz that is the center frequency of the PCT (Personal Communication Telephone) system. When the transmitted power from the base station is fixed at *20* mW, and the gain of the mobile antenna is assumed to be unity in dimensionless, by utilizing the well-

known Friis transmission equation [12], the relationship of power received by the mobile antenna (P_r) is

$$P_r = EIRP \cdot G_r \cdot (\frac{\lambda}{4\pi R})^2, \quad (3)$$

where *EIRP* stands for Effective Isotropic Radiated Power which is the product of the transmitted power and the directive gain of the base-station antenna, G_r is the gain of the mobile antenna (unity in dimensionless), λ is the operating wavelength (m) and R is the communication range (m).

As the mobile unit moves along the road from *A* to *B* and so on until to *F* as shown in Fig.6.10 (not to scale).

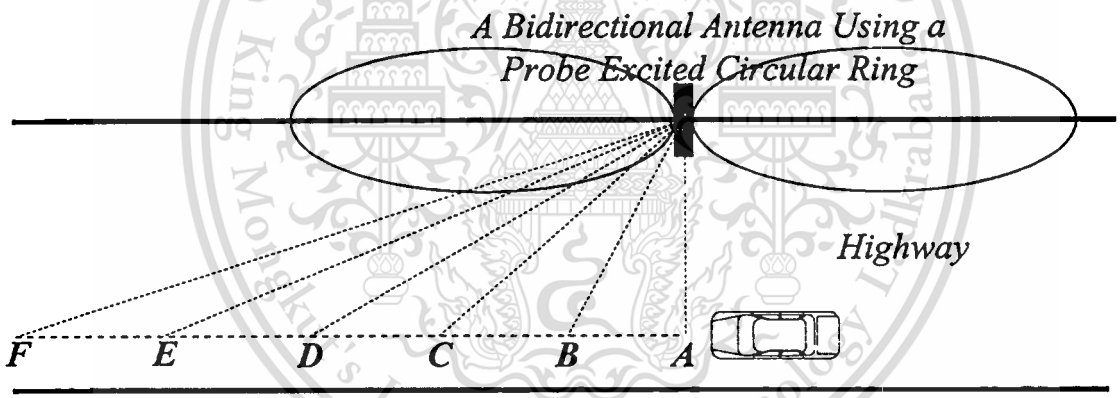

Fig 6.10 Antenna coverage on the highway (not to scale)

The directive gain is slightly changed; however, the received signal is considerably changed according to the different distances. Table II show received signal at those different positions.

Table 6.1 Estimation of communication range

Position	Directive Gain (dBi)	Distance (m)	EIRP (dB_W)	Field Strength ($dB_{\mu V}$)
A	*0*	-	-	-
B	*5.3*	*100*	*-11.7*	*25.1*
C	*5.8*	*300*	*-11.2*	*20.6*
D	*6.2*	*600*	*-10.8*	*17.8*
E	*6.5*	*1200*	*-10.5*	*14.9*
F	*6.7*	*2400*	*-10.3*	*12.0*

We can realize that, for a conventional receiver with *12* $dB_{\mu V}$ sensitivity, the maximum range is around *2.4* km. The maximum range in case of the *2.15* dBi omnidirectional antenna is employed in place of the bidirectional one is also calculated. It should be pointed out that the maximum range of the proposed bidirectional antenna is twice longer than that of the system that employs the omnidirectional antenna. In order to yield more accurate result, at least 2-ray model considering ground reflection shall be considered, that is left for further study.

6.5 Conclusion

According to the design curve, the ring width can be designed for a specific ring radius and directivity. This designed curve shows that this antenna can provide directivity in excess of *7* dBi. Experimental results indicate that the antenna has radiation characteristics as proposed. Radiation patterns in E-plane have good agreement whereas those in the H-plane have some different due to neglecting mutual coupling and edge effect in calculation. This result in slightly reduced in antenna gain. It was shown that this antenna could be matched simply by choosing appropriate

probe length. It enhances the communication range in the PCT system to twice of the system employed a conventional omnidirectional antenna.

Chapter 7

Conclusions and Discussions

A simple, compact and low cost bidirectional antenna with moderate gain to be used in a specific narrow region in a mobile communication system such as express way, corridor, tunnel and etc., is required. It can reduce the number of base stations and the installation budget.

The author proposed a bidirectional antenna using a probe excited ring to support the above requirement. The principle of the antenna is to employ a ring to compress electromagnetic energy from an omnidirectional pattern of a probe to two opposite directions. It is initially described theoretically in term of a bidirectional antenna using a probe excited rectangular ring. Radiation characteristics of the antenna can be considered from the Dyadic Green's function to find electric field inside the ring, on the apertures and radiation from the antenna, respectively. Then input impedance is investigated by using induced EMF method. This principle is summarized in chapter 2.

Numerical results which describe the analysis of a bidirectional antenna using a probe excited rectangular ring are addressed in chapter 3. They confirm that the bidirectional pattern can be achieved simply when the proper antenna dimensions are chosen. It was pointed out that this antenna could provide directivity in excess of *6* dBi.

Chapter 4 mentions about the design of a bidirectional antenna using a probe excited rectangular ring. Characteristics of a prototype antenna are illustrated and proved to be satisfactory. However, in a viewpoint of manufacturing process, a circular ring can be easier fabricated. Therefore, it is significant to investigate a bidirectional

antenna using probe excited circular ring. To carry out this investigation, a principle of a bidirectional antenna using a probe excited rectangular ring is applied.

Chapter 5 describes principle of a bidirectional antenna using a probe excited circular ring. Its ring radius and length are properly chosen to let only the dominant wave accommodates inside the ring and the maximum directivity is achieved.

The design and prototype fabrication at the frequency of *1.9* GHz (the operating frequency of the PCT system) is shown. Measured results show that this antenna possesses gain of *5.4* dBi over the bandwidth of *17* %, which is sufficient for the system requirement. Furthermore, communication range estimation is conducted. It was found that this antenna can extend the twice range than that of the conventional omnidirectional antenna. The materials related to these topics are shown in chapter 6.

As the aforementioned earlier, it is obvious that a bidirectional antenna using a probe excited ring is satisfactorily developed. It is significant to the mobile communication in narrow space such as express way, corridor, tunnel and etc. However, there are many interesting topics to be considered such as edge effect and mutual coupling at the apertures, development of polarization diversity of this antenna to mitigate multipath fading, array of this antenna with simple feed to increase its gain, etc. These topics are left for further study. The proposed antennas about 1,000 pieces have been installed on the elevated highway in the city of Bangkok.

References

[1] L.C. Godara, "Applications of antenna array to mobile communications part I performance improvement, feasibility, and system considerations," *Proc. IEEE*, vol.85, no.7, pp.1031-1060, July 1997.

[2] R.C. Johnson and H. Jasik, "Antenna Engineering Handbook," McGraw-Hill Inc., 1984.

[3] K. Cho and T. Hori, "Bidirectional rod antenna composed of narrow patches," *Proc. IEEE Antennas Propagat. Soc. Int. Symp.*, pp.174-177, June 1994.

[4] T. Hori, K. Cho, and K. Kagoshima, "Bidirectional base station antenna illuminating a street microcell for personal communication system," *Proc. 9th Inst. Elect. Eng. Conf. Antennas Propagat.*, pp.419-422, Apr.1995.

[5] H. Arai and K. Kohzu, "A bidirectional notch antenna," *Proc. IEEE Antennas Propagat. Soc. Int. Symp.*, pp.42-45, July 1996.

[6] K. Kohzu and H. Arai, "Dual band bidirectional antenna," *Proc. 1996 Asia-Pacific Microwave Conf.*, pp.856-859, Dec. 1996.

[7] T. Mukaiyama, H. Arai, and Y. Ebine, "Bi-directional notch and crank-shaped antenna," *Proc. 1997 Asia-Pacific Microwave Conf.*, pp.417-420, Dec. 1997.

[8] S. Kosulvit, C. Phongcharoenpanich, M. Krairiksh, and T. Wakabayashi, "Radiation characteristics of a bidirectional antenna using a linear probe in rectangular ring," *Proc. 1998 Int. Conf. on Microwave and Millimeter Wave Technology*, pp.337-340, Aug. 1998.

[9] S. Kosulvit, C. Phongcharoenpanich, M. Krairiksh, and T. Wakabayashi, "Evaluation of input impedance a bidirectional

antenna using a linear probe in rectangular ring," *Proc. of the 5th Int. Sym. on Antenna, Propagation and Electromagnetic Theory*, Beijing pp.650-653, Aug. 2000

[10] C.A. Balanis, "Advanced Engineering Electromagnetics," John Wiley & Sons, Inc., 1998

[11] R.E. Collin, "Antennas and Radiowave Propagation," McGraw-Hill International Editions, 1985

[12] C.A. Balanis, "Antenna Theory Analysis and Design," 2nd ed. John Wiley & Sons, Inc., 1997

[13] R.F. Harrington, "Time-Harmonic Electromagnetic Fields," McGraw-Hill, New York, 1961

[14] S. Kosulvit, C. Phongcharoenpanich, M. Krairiksh, and T. Wakabayashi, "Radiation characteristics of a bidirectional antenna using a probe excited circular ring," *Proc. 1999 IEEE Int. Symp. on Intelligent Signal Processing and Communication Systems*, pp.713--716, Dec. 1999.

[15] S. Kosulvit, C. Phongcharoenpanich, M. Krairiksh, and T. Wakabayashi, "Design of a bidirectional antenna using a probe excited circular ring," *Proc. 1999 Thailand-Japan Joint Symp. on Microwaves*, pp.55-59, Sep. 1999.

[16] S. Kosulvit, M. Krairiksh, C. Phongcharoenpanich, and T. Wakabayashi, "A simple and cost-effective bidirectional antenna using a probe excited circular ring," *IEICE Trans. Electronics*: vol. E84-C, no.4, pp.443-450, Apr. 2001.

[17] N. Marcuvitz, "Waveguide Handbook," Dover, 1951.

[18] K.F. Sander and G. A. L. Reed, "Transmission and Propagation of Electromagnetic Waves," Cambridge University Press, 1986.

Related Publications

[1] S. Kosulvit, C. Phongcharoenpanich, M. Krairiksh, and T. Wakabayashi, "Radiation characteristics of a bidirectional antenna using a linear probe in rectangular ring," *Proc. 1998 Int. Conf. on Microwave and Millimeter Wave Technology*, pp.337-340, Aug. 1998.

[2] S. Kosulvit, C. Phongcharoenpanich, M. Krairiksh, and T. Wakabayashi, "Design of a bidirectional antenna using a probe excited circular ring," *Proc. 1999 Thailand-Japan Joint Symp. on Microwaves*, pp.55-59, Sep. 1999.

[3] S. Kosulvit, C. Phongcharoenpanich, M. Krairiksh, and T. Wakabayashi, "Radiation characteristics of a bidirectional antenna using a probe excited circular ring," *Proc. 1999 IEEE Int. Symp. on Intelligent Signal Processing and Communication Systems*, pp.713-716, Dec. 1999.

[4] S. Kosulvit, C. Phongcharoenpanich, M. Krairiksh, and T. Wakabayashi, "Evaluation of input impedance a bidirectional antenna using a linear probe in rectangular ring," *Proc. of the 5th Int. Sym. on Antennas, Propagation and Electromagnetic Theory*, Beijing pp.650-653, Aug. 2000

[5] S. Kosulvit, M. Krairiksh, C. Phongcharoenpanich, and T. Wakabayashi, "A simple and cost-effective bidirectional antenna using a probe excited circular ring," *IEICE Trans. Electronics*: vol. E84-C, no.4, pp.443-450, Apr. 2001.

Author Biography

Sompol Kosulvit was born in Ubonrachathani. He received B.Eng. and M.Eng. from Tokai University. He is currently an assistant professor at Department of Telecommunication Engineering, Faculty of Engineering, King Mongkut's Institute of Technology Ladkrabang (KMITL), and serves as the assistant leader of Wireless Communication Laboratory, Research Center for Communications and Information Technology at the same institute. His research interests are antenna for mobile communications and microwave applications.